Electronic Supplementary Information

New half-sandwich ruthenium(II) complexes as proteosynthesis inhibitors in cancer cells

Francisco J. Ballester,[a,+] Enrique Ortega,[a,+] Vanesa Porto,[b] Hana Kostrhunova,[c] Nerea Dávila,[b] Delia Bautista,[d] and Viktor Brabec,[c] Fernando Domínguez,[b,*] M. Dolores Santana,[a,*] and José Ruiz [a,*]

[a] Departamento de Química Inorgánica and Regional Campus of International Excellence "Campus Mare Nostrum", Universidad de Murcia, and Biomedical Research Institute of Murcia (IMIB-Arrixaca), E-30071 Murcia, Spain Tel: + 34 868887455, Email: jruiz@um.es; dsl@um.es.

[b] CIMUS, Universidad de Santiago de Compostela, Avenida Barcelona s/n, 15782, Santiago de Compostela, Spain. Email: fernando.dominguez@usc.es

[c] Institute of Biophysics, Academy of Sciences of the Czech Republic, v.v.i., Kralovopolska 135, 612 65 Brno, Czech Republic.

[d] SAI, Universidad de Murcia, E-30071-Murcia, Spain

[+] These authors contributed equally to this work.

TABLE OF CONTENTS

STARTING MATERIAL AND REAGENTS 3
INSTRUMENTATION 3
SYNTHESIS AND CHARACTERIZATION OF RUTHENIUM COMPOUNDS 4
NMR SPECTRA OF COMPOUNDS 1a-3b 9
HPLC PURITY ANALYSES 22
STUDIES OF INTERACTION WITH OXIDATIVE BIOMOLECULES 28
HYDROLYSIS STUDIES 31
X-RAY CRYSTALLOGRAPHIC ANALYSIS 34
REACTION WITH HUMAN SERUM ALBUMIN (HSA) 39
CELL LINES AND CULTURE 44
CYTOTOXICITY ASSAYS 44
METAL ACCUMULATION 45
MITOCHONDRIAL POLARIZATION ASSAY 45
APOPTOTIC INDUCTION ASSAY 47
FLUORESCENCE DETECTION OF CASPASE 3/7 ACTIVATION 48
ROS INDUCTION ASSAY 49
REAL-TIME CELL ELECTRONIC SENSING 51
PROTEIN SYNTHESIS INHIBITION ASSAY 52
FLOW CYTOMETRIC CELL CYCLE ANALYSIS 53
QUANTITATIVE-PCR (QPCR) 54
DNA DAMAGE ASSAY: PH2AX DETECTION 54
SUPEROXIDE LEVELS 55
REFERENCES 56

Starting material and reagents

All synthetic manipulations were carried out under an atmosphere of dry, oxygen-free nitrogen using standard Schlenk techniques. Solvents were dried by the usual methods. Organic ligands, magnesium sulfate, sodium acetate, dimethyl sulfoxide (DMSO) and CDDP were obtained from Sigma-Aldrich (Madrid, Spain) and ruthenium compounds from Johnson Matthey. Deuterated solvents were obtained from Euriso-top.

For cellular studies, stock solutions were prepared by dissolving the compounds in DMSO to a final concentration of 20 mM and serially diluted prior to testing in DMSO. The final DMSO concentration in culture medium did not exceed 0.4 % (v/v) to avoid DMSO toxicity. CDDP stock solution was prepared by dissolving CDDP in ultrapure water (Milli-Q®, Merck Millipore) to a final concentration of 20 mM.

Instrumentation

The ^{1}H and ^{13}C NMR spectra were recorded on Bruker AC 300E, Bruker AV 400, or Bruker AV 600 NMR spectrometer. Chemical shifts are cited relative to $SiMe_4$ and were determined by reference to the residual ^{1}H and ^{13}C solvent peaks. The complexes were analyzed via multinuclear 2D (^{1}H-^{1}H COSY and ^{1}H-^{13}C HSQC) NMR spectroscopic experiments that allowed unambiguous assignments of all resonances. UV/vis spectroscopy was carried out on a PerkinElmer Lambda 750 S spectrometer with operating software. ESI mass (positive mode) analyses were performed on a HPLC/MS TOF 6220. The isotopic distribution of the heaviest set of peaks matched very closely that calculated for the formulation of the complex cation in every case. The FT-IR spectra were recorded on a Perkin-Elmer 1430 spectrophotometer using Nujol mulls between polyethylene sheets. The C, H, N and S analyses were performed with a Carlo Erba model EA 1108 microanalyzer.

Synthesis and characterization of ruthenium compounds

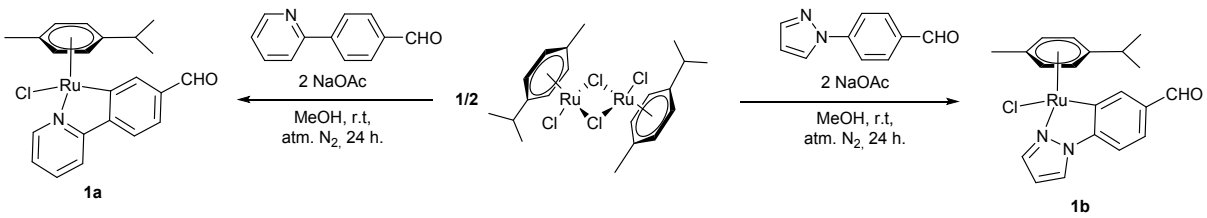

Scheme S1 The synthetic protocols of half-sandwich complexes **1a** and **1b**.

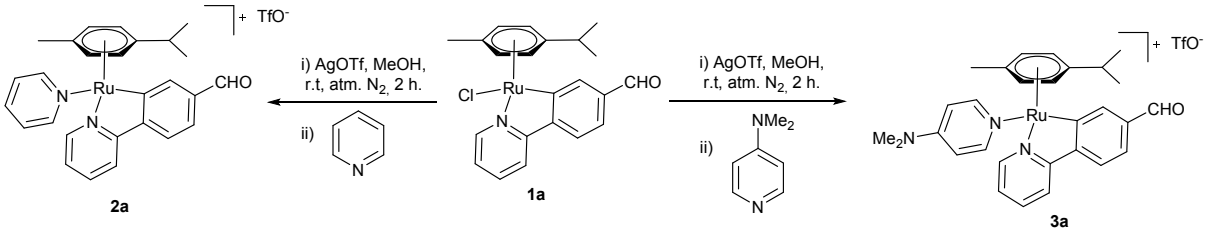

Scheme S2 The synthetic protocols of complexes **2a** and **3a**.

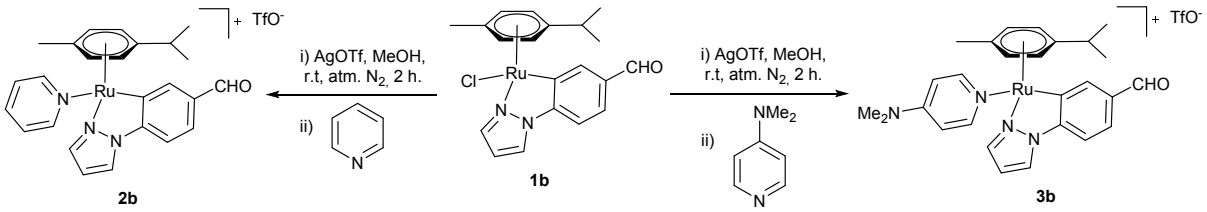

Scheme S3 The synthetic protocols of complexes **2b** and **3b**.

Synthesis of [(η^6-*p*-cymene)Ru(ppy-CHO)Cl] (1a)

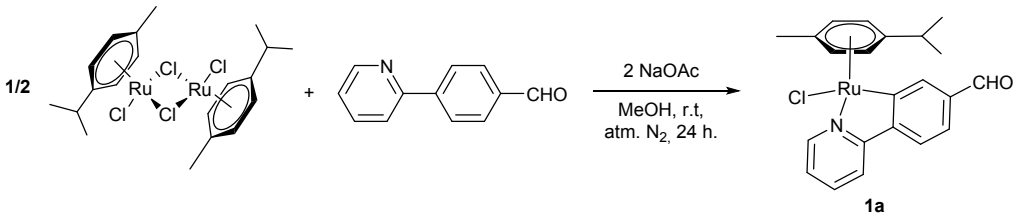

1a

4-(Pyridin-2-yl)benzaldehyde (0.8 mmol) was dissolved in methanol (20 mL) under nitrogen atmosphere then sodium acetate (1.6 mmol) and ruthenium dimer [(η^6-*p*-cymene)$RuCl_2]_2$ (0.4 mmol) were added with constant stirring. The solution was stirred at room temperature under dark for 24 h after that an orange solid was obtained. The solid was filtered, washed with diethyl ether and dried under vacuum. Yield: 79%. ESI-MS (pos ion mode, DMSO): *m/z* = 418.0751 $[M –Cl]^+$. **^{1}H NMR (401 MHz, CD_3CN, 25 °C)** δ (ppm): 10.08 (s, H_8), 9.38 (d, *J* = 5.4 Hz, H_7), 8.65 (d, *J* = 1.5 Hz, H_1), 7.97 (d, *J* = 7.5 Hz, H_3), 7.88 (m, $2H_{4+5}$), 7.52 (dd, *J* = 7.8, 1.5 Hz, H_2), 7.27 (m, H_6), 5.75 (m, 2H), 5.37 (dd, *J* = 6.4, 1.2 Hz, 1H), 5.12 (dd, *J* = 6.0, 1.2 Hz, 1H), 2.33 (sept, *J* = 6.9 Hz, 1H), 2.02 (s, 3H), 0.91 (d, *J* = 6.9 Hz, 3H), 0.80 (d, *J* = 6.9 Hz, 3H). **^{13}C NMR (101 MHz, CD_2Cl_2, 25 °C)** δ (ppm): 193.57, 182.32, 164.05, 155.47, 149.67, 141.64, 137.43, 136.09, 124.00, 123.64, 123.21, 120.37, 102.41, 101.31, 91.68, 90.12, 84.95, 82.37, 31.24, 22.56, 21.76, 18.92. IR (Nujol, cm^{-1}): ν(CO) = 1681, ν(Ru-Cl) 277. Anal. Calcd for $C_{22}H_{22}ClNORu$ (452.94): C, 59.03; H, 5.38; N, 2.99; Found: C, 58.71; H, 5.39; N, 3.17 (%).

[(η^6-*p*-cymene)Ru(ppz-CHO)Cl] (1b)

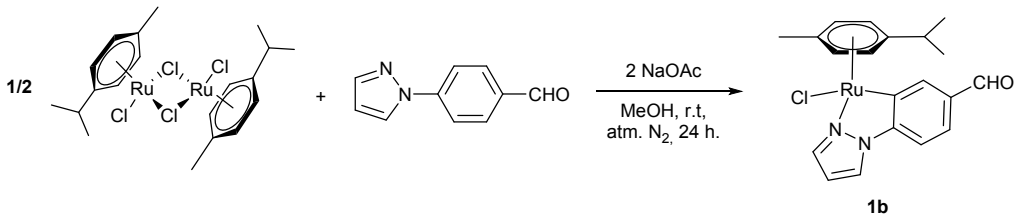

1b

The procedure used was similar to that described for **1a**, using 4-(1H-pyrazol-1-yl)benzaldehyde. The solution was stirred at room temperature under dark for 24 h then the reaction mixture was concentrated under reduced pressure and a orange solid precipitated that was collected by filtration, washed with diethyl ether and dried under vacuum. Yield: 76%. ESI-MS (pos ion mode, DMSO): *m/z* = 407.0699 $[M –Cl]^+$.

^{1}H NMR (401 MHz, CD_3CN, 25 °C) δ (ppm): 10.03 (s, H_7), 8.67 (d, J = 2.0 Hz, H_1), 8.26 (m, $2H_{4+6}$), 7.57 (dd, J = 8.0, 1.6 Hz, H_2), 7.47 (d, J = 8.4 Hz, H_3), 6.63 (dd, J = 2.8, 2.4 Hz, H_5), 5.74 (dd, J = 5.6, 0.8 Hz, 1H), 5.71 (dd, J = 5.6, 0.8 Hz, 1H), 5.46 (dd, J = 6.0, 0.8 Hz, 1H), 5.20 (dd, J = 6.0, 1.2 Hz, 1H), 2.33 (sept, J = 6.8 Hz, 1H), 2.01 (s, 3H), 0.90 (d, J = 6.8 Hz, 3H), 0.85 (d, J = 6.8 Hz, 3H). **^{13}C NMR (101 MHz, CD_3CN, 25 °C)** δ (ppm): 193.58, 164.48 (s), 147.84 (s), 144.98, 143.09, 134.54 (s), 127.85, 126.07, 112.58, 110.28, 102.48 (s), 100.88 (s), 90.29, 89.09, 85.51, 82.75, 31.49, 22.43, 22.04, 18.91. IR (Nujol, cm^{-1}): ν(CO) = 1679, ν(Ru-Cl) 281. Anal. Calcd for $C_{20}H_{21}ClN_2ORu$ (441.92): C, 54.36; H, 4.79; N, 6.34; Found: C, 54.17; H, 4.65; N, 6.30 (%).

[(η^6-*p*-cymene)Ru(ppy-CHO)(py)][CF_3SO_3] (**2a**)

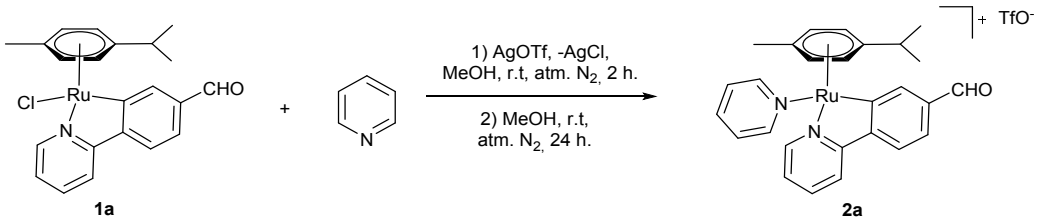

[(η^6-*p*-cymene)Ru(ppy-CHO)Cl] (**1a**) (0.13 mmol) was dissolved in methanol (20 mL) under nitrogen atmosphere then silver trifluoromethanesulfonate (0.13 mmol) was added with constant stirring. After stirring at room temperature for 2 h, the reaction solution was filtered. Pyridine (0.13 mmol) was added to the filtrate and the mixture was stirred for 24 h at room temperature. After removal the solvent, the residue was dissolved in CH_2Cl_2 and precipitated by n-hexane. The green solid was collected by filtration, washed with n-hexane and dried under vacuum. Yield: 97%. ESI-MS (pos ion mode, DMSO): m/z = 418.0744 [M^+ –py]. **^{1}H NMR (401 MHz, CD_3CN, 25 °C) δ (ppm)**: 10.18 (s, H_8), 9.55 (dd, J = 6.0, 0.8 Hz H_7), 8.90 (d, J = 1.5 Hz, H_1), 8.39 (dd, J = 5.2, 1.6 Hz, $2H_9$), 7.96 (m, $2H_{4+5}$), 7.82 (d, J = 8.0 Hz, H_3), 7.71 tt, , J = 7.6, 1.6 Hz, H_{11}), 7.63 (dd, J = 8.0, 1.6 Hz, H_2), 7.48 (td, J = 6.0, 2.4 Hz, H_6), 7.20 (m, $2H_{10}$), 6.11 (m, 2H), 5.79 (dd, J = 6.0, 1.2 Hz, 1H), 5.37 (dd, J = 6.0, 1.2 Hz, 1H), 1.64 (s, 3H), 0.81 (d, J = 6.8 Hz, 2H), 0.74 (d, J = 6.8 Hz, 3H). **^{13}C NMR (101 MHz, CD_3CN, 25 °C)** δ (ppm): 194.37, 180.27, 165.02, 157.02, 155.05, 150.84, 142.39, 140.01, 139.54, 138.00, 126.53, 125.78, 125.51, 125.21, 121.82, 106.65, 102.15, 93.92, 93.81, 91.08, 83.09, 31.72, 22.62, 22.14, 18.18. HPLC purity: > 99%. IR (Nujol, cm^{-1}): ν(CO) 1682. Anal. Calcd for $C_{28}H_{27}F_3N_2O_4SRu$ (645.66): C, 52.09; H, 4.22; N, 4.34; S, 4.14; Found: C, 51.73; H, 4.42; N, 4.41; S, 4.02 (%).

[(η^6-*p*-cymene)Ru(ppy-CHO)(NMe$_2$py)][CF$_3$SO$_3$] (3a).

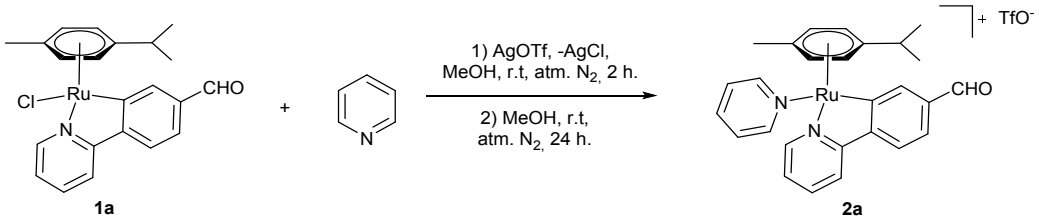

1a 2a

The procedure used was similar to that described for **2a**, using N,N-dimethylpyridin-4-amine (NMe$_2$py). Yellow solid. Yield: 83%. ESI-MS (pos ion mode, DMSO): *m/z* = 540.1583 [M]$^+$. **^{1}H NMR (300 MHz, CD$_3$CN, 25 °C)** δ (ppm): 10.16 (s, H$_8$), 9.51 (d, *J* = 7.6 Hz, H$_7$), 8.86 (d, *J* = 2.0 Hz, H$_1$), 7.95 (d, *J* = 4.8 Hz, 2H$_{4+5}$), 7.82 (d, *J* = 10.8 Hz, H$_3$), 7.72 (dd, *J* = 8.0, 1.6 Hz, 2H$_9$), 7.61 (dd, *J* = 10.8, 2.0 Hz, H$_2$), 7.44 (dt, *J* = 7.6, 6.0 Hz, H$_6$), 6.27 (m, 2H$_{10}$), 6.04 (m, 2H), 5.73 (d, *J* = 8.4 Hz 1H), 5.32 (d, *J* = 8.0 Hz, 1H), 2.86 (s, 6H$_{11}$), 1.70 (s, 3H), 0.81 (d, *J* = 6.9 Hz, 3H), 0.75 (d, *J* = 6.9 Hz, 3H). **^{13}C NMR (75 MHz, CD$_3$CN, 25 °C)** δ (ppm): 194.30, 181.31(s), 164.97(s), 156.88, 155.34(s), 153.12, 150.72(s), 142.24, 139.70, 137.76(s), 125.39, 125.23, 125.10, 121.61, 108.74, 106.50(s), 101.90(s), 93.61, 93.24, 90.66, 82.66, 39.36, 31.76, 22.68, 22.23, 18.41. HPLC purity: > 99%. IR (Nujol, cm^{-1}): ν(CO) 1682. Anal. Calcd for C$_{30}$H$_{32}$F$_3$N$_3$O$_4$SRu (688.73): C, 52.91; H, 5.01; N, 5.97; S, 4.56; Found: C, 51.73; H, 4.71; N, 6.02; S, 4.43 (%).

[(η^6-*p*-cymene)Ru(ppz-CHO)py][CF$_3$SO$_3$] (2b)

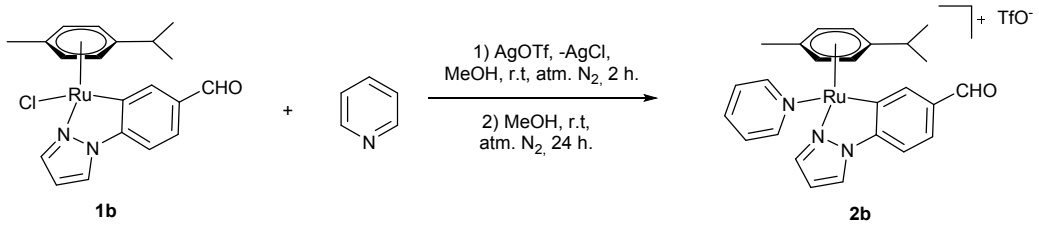

1b 2b

The procedure used was similar to that described for **2a**, using **1b** as starting material. Green solid. Yield: 87%. ESI-MS (pos ion mode, DMSO): *m/z* = 407.0707 [M$^+$ –py]. **^{1}H NMR (401 MHz, CD$_3$CN, 25 °C)** δ (ppm): 10.11 (s, H$_7$), 8.90 (d, *J* = 2.0 Hz, H$_1$), 8.58 (dd, *J* = 2.0, 0.4 Hz, H$_6$), 8.34 (m, 2H$_9$), 8.28 (dd, *J* = 3.2, 0.8 Hz, H$_4$), 7.71 (tt, *J* = 7.6, 1.6 Hz, H$_{10}$), 7.66 (dd, *J* = 8.0, 1.6 Hz, H$_2$), 7.44 (d, *J* = 8.0 Hz, H$_3$), 7.17 (m, 2H$_8$), 6.74 (dd, *J* = 2.8, 2.0 Hz, H$_5$), 6.08 (dd, *J* = 6.4 Hz, 1.2, 1H), 6.03 (dd, *J* = 6.0, 1.2 Hz, 1H), 5.81 (dd, *J* = 6.0, 1.2 Hz, 1H), 5.43 (dd, *J* = 6.0, 1.2 Hz, 1H), 1.62 (s, 3H), 0.77 (d, *J* = 7.2 Hz, 3H), 0.75 (d, *J* = 7.2 Hz, 3H).

^{13}C NMR (151 MHz, CD_3CN, 25 °C) δ (ppm): 193.31, 162.05, 155.02, 147.68, 146.55, 143.10, 139.65, 135.79, 129.50, 127.58, 126.50, 113.21, 111.19, 106.34, 101.91, 92.26, 92.21, 89.77, 83.03, 31.49, 22.43, 22.26, 18.12. HPLC purity: > 99%. IR (Nujol, cm-1): ν(CO) 1679. Anal. Calcd for C26H26F3N3O4SRu (634.64): C, 49.21; H, 4.13; N, 6.62; S, 5.05; Found: C, 48.87; H, 4.13; N, 6.45; S, 4.77 (%).

[(η^6-*p*-cymene)Ru(ppz-CHO)(NMe_2py)][CF_3SO_3] (3b)

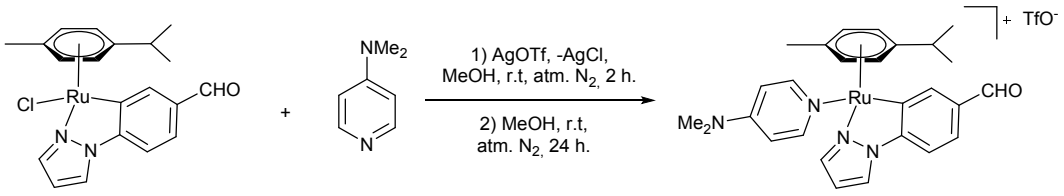

The procedure used was similar to that described for 2b, using N,N-dimethylpyridin-4-amine (ampy). Green solid. Yield: 47%. ESI-MS (pos ion mode, DMSO): *m/z* = 529.1553 $[M]^+$. **^{1}H NMR (401 MHz, CD_3CN, 25 °C)** δ (ppm): 10.10 (s, H_7), 8.86 (d, *J* = 1.6 Hz, H_1), 8.53 (d, *J* = 2.0 Hz, H_6), 8.28 (d, *J* = 2.8 Hz, H_4), 7.66 (m, $3H_{8+2}$), 7.45 (d, *J* = 8.0 Hz, H_3), 6.72 (m, H_5), 6.29 (d, *J* = 7.2, $2H_9$), 6.02 (d, *J* = 5.6 Hz, 1H), 5.98 (d, *J* = 5.6 Hz, 1H), 5.77 (d, *J* = 6.0 Hz, 1H), 5.39 (d, *J* = 5.6 Hz, 1H), 2.87 (s, $6H_{10}$), 1.69 (s, 3H), 0.79 (d, *J* = 6.8 Hz, 3H), 0.77 (d, *J* = 6.8 Hz, 3H). **^{13}C NMR (101 MHz, CD_3CN, 25 °C)** δ (ppm): 193.32, 162.92 (s), 155.41 (s), 153.01, 147.60 (s), 146.14, 142.86, 142.32 (s), 135.51 (s), 129.06, 127.35, 117.35 (s), 112.98, 110.95, 108.65, 106.11 (s), 101.62 (s), 91.91, 91.57, 89.21, 82.50, 39.32, 31.46, 22.46, 22.29, 18.28. HPLC purity: > 99%. IR (Nujol, cm-1): ν(CO) 1679. Anal. Calcd for $C_{28}H_{31}F_3N_4O_4SRu$ (677.71): C, 49.26; H, 4.61; N, 8.27; S, 4.74; Found: C, 49.03; H, 4.55; N, 7.96; S, 4.45 (%).

NMR Spectra of compounds 1a-3b

Compound 1a

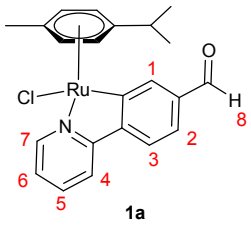

1a

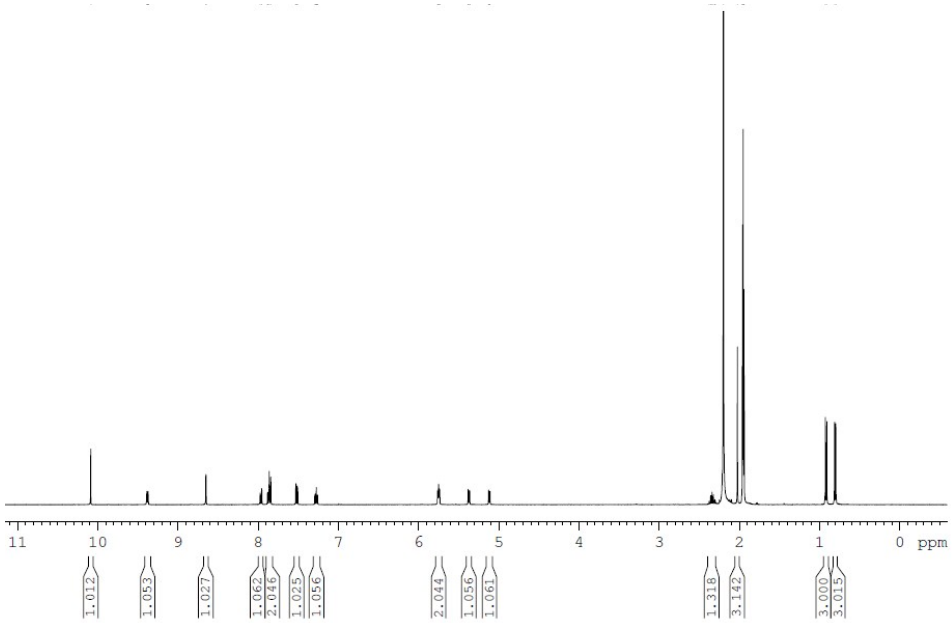

Figure S1. ^{1}H NMR spectrum of complex **1a** (in CD_3CN solution at 25 °C).

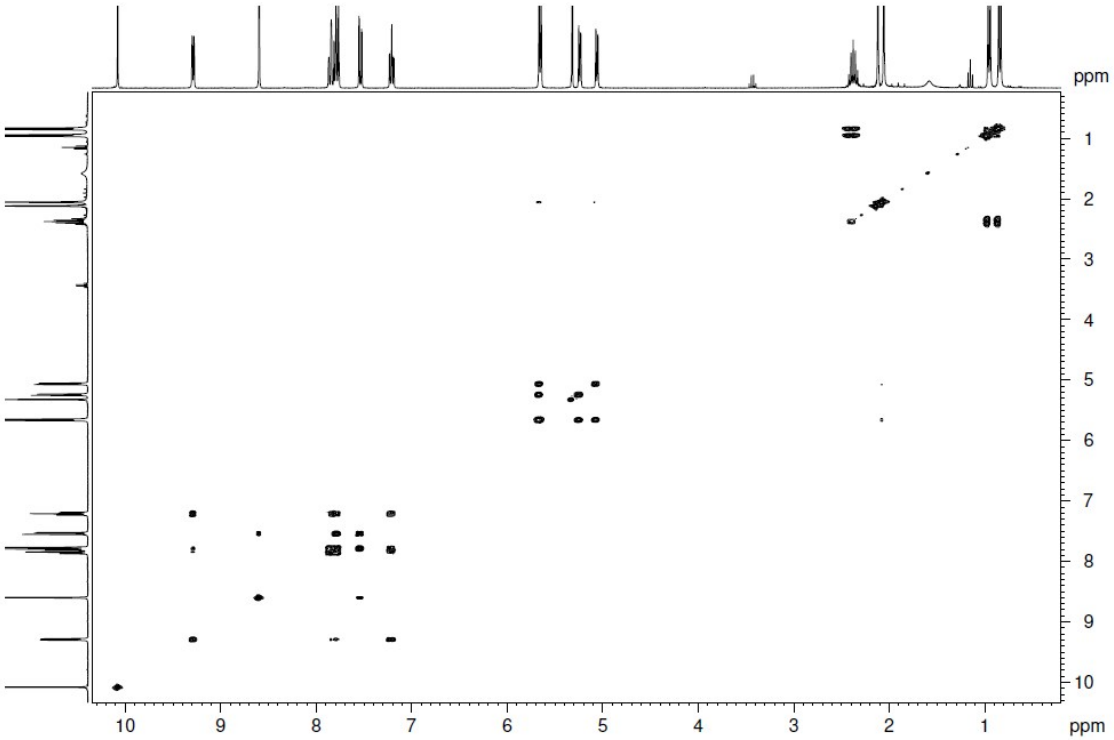

Figure S2. {^{1}H-^{1}H} COSY spectrum of complex **1a** (in CD_2Cl_2 solution at 25 °C).

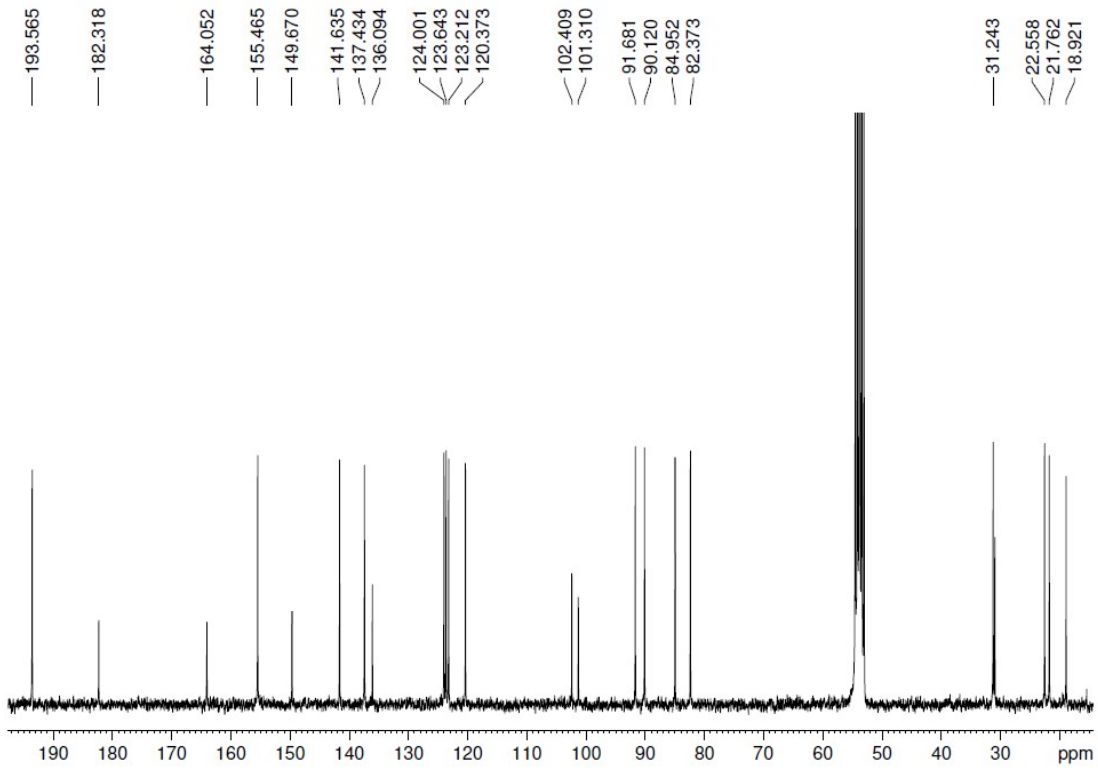

Figure S3. ^{13}C NMR spectrum of complex **1a** (in CD_2Cl_2 solution at 25 °C).

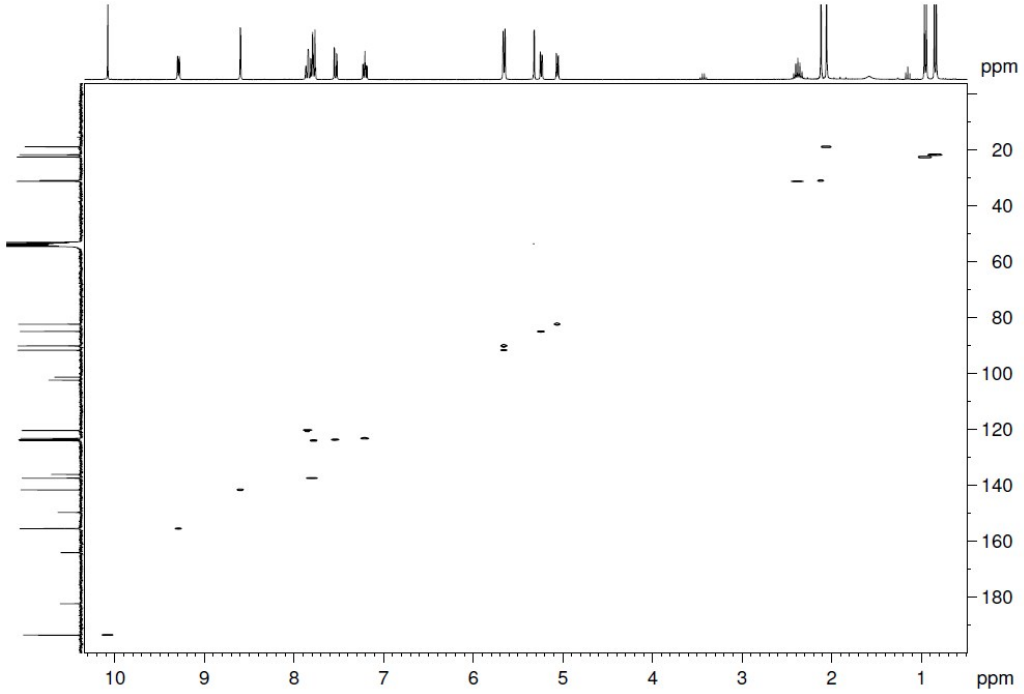

Figure S4. {^{1}H – ^{13}C} HSQC spectrum of complex **1a** (CD_2Cl_2 25 °C).

Compound 1b

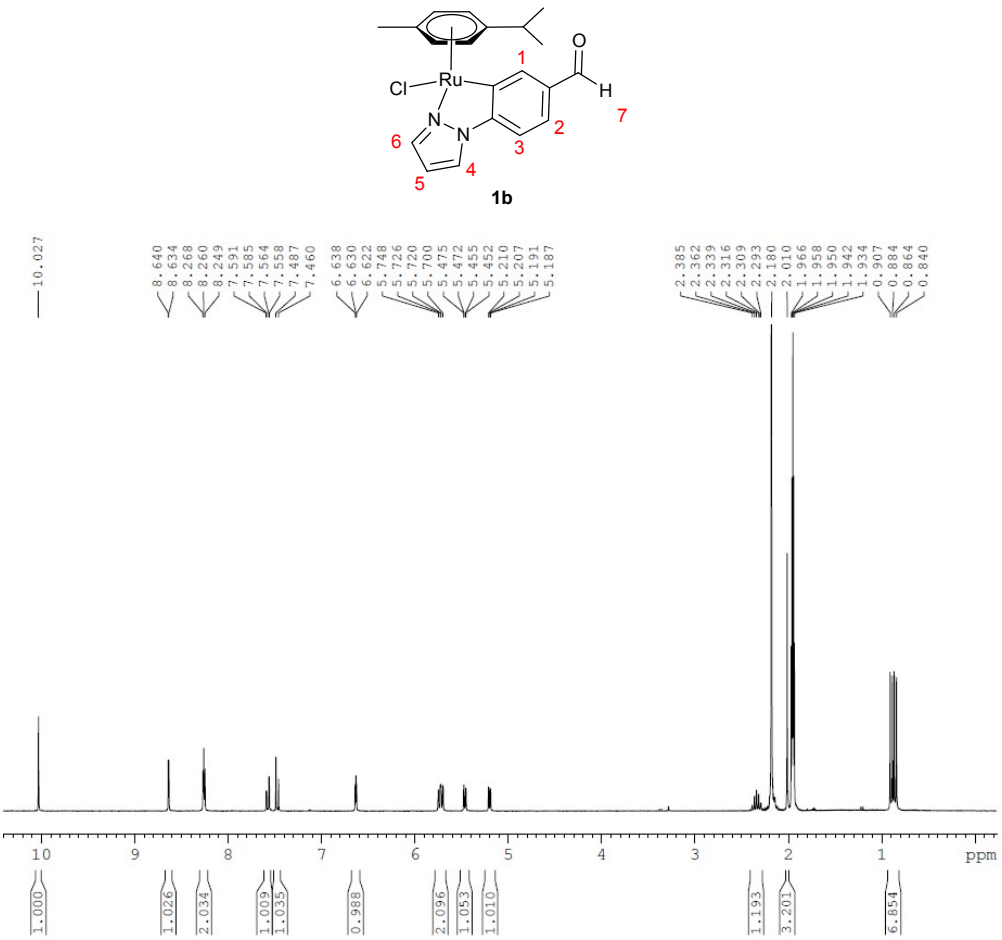

Figure S5. ^{1}H NMR spectrum of complex **1b** (in CD_3CN solution at 25 °C).

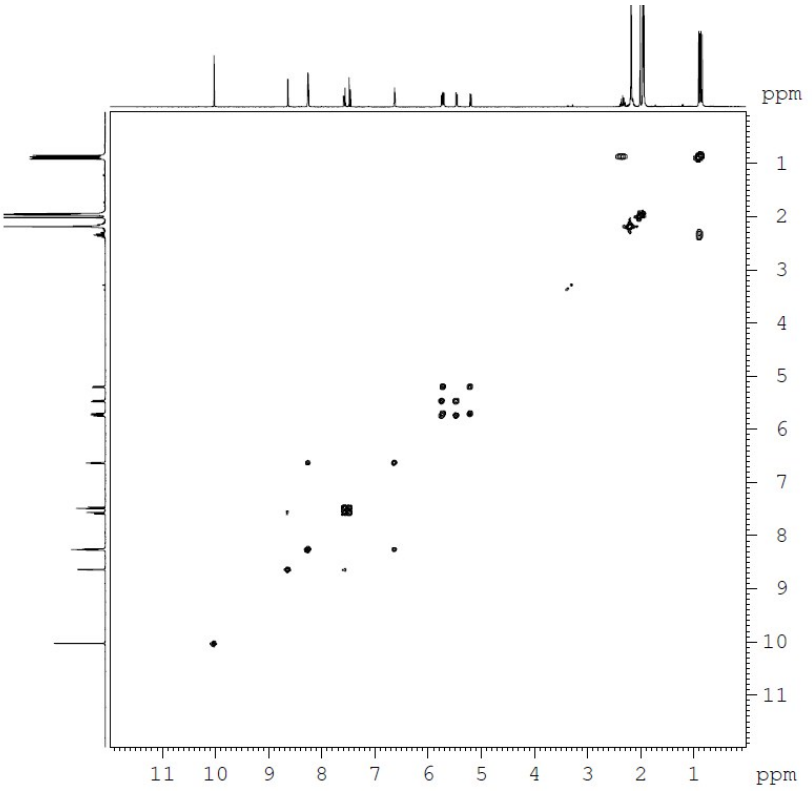

Figure S6. {^{1}H-^{1}H} COSY spectrum of complex **1b** (in CD_3CN solution at 25 °C).

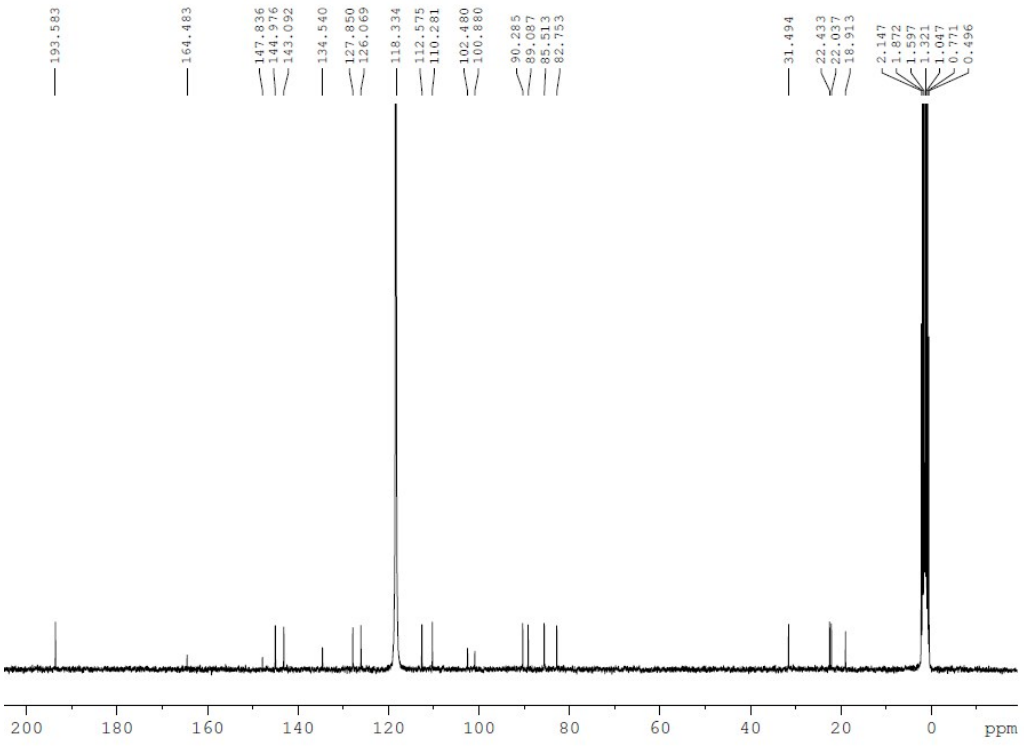

Figure S7. ^{13}C NMR spectrum of complex **1b** (in CD_3CN solution at 25 °C).

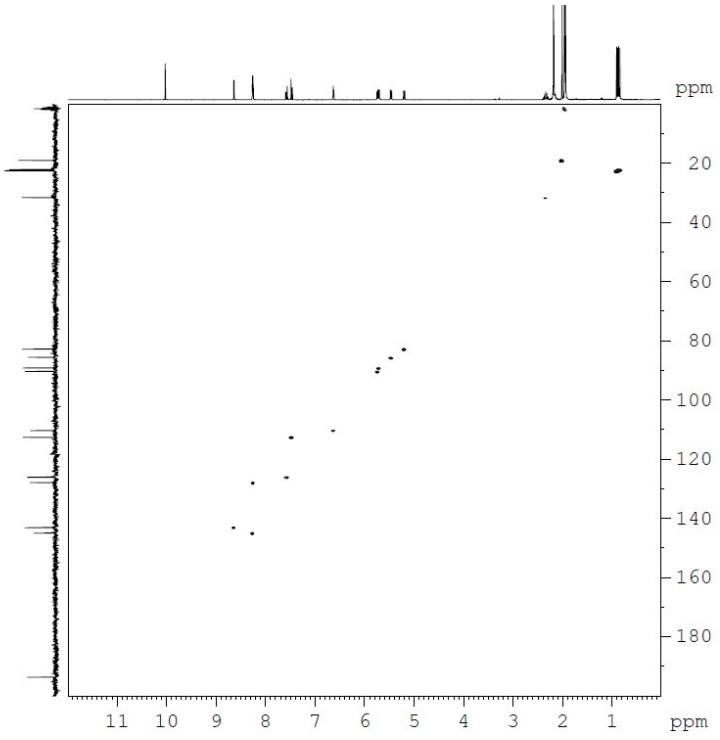

Figure S8. $\{^1H - ^{13}C\}$ HSQC spectrum of complex **1b** (CD_3CN, 25 °C)

Compound 2a

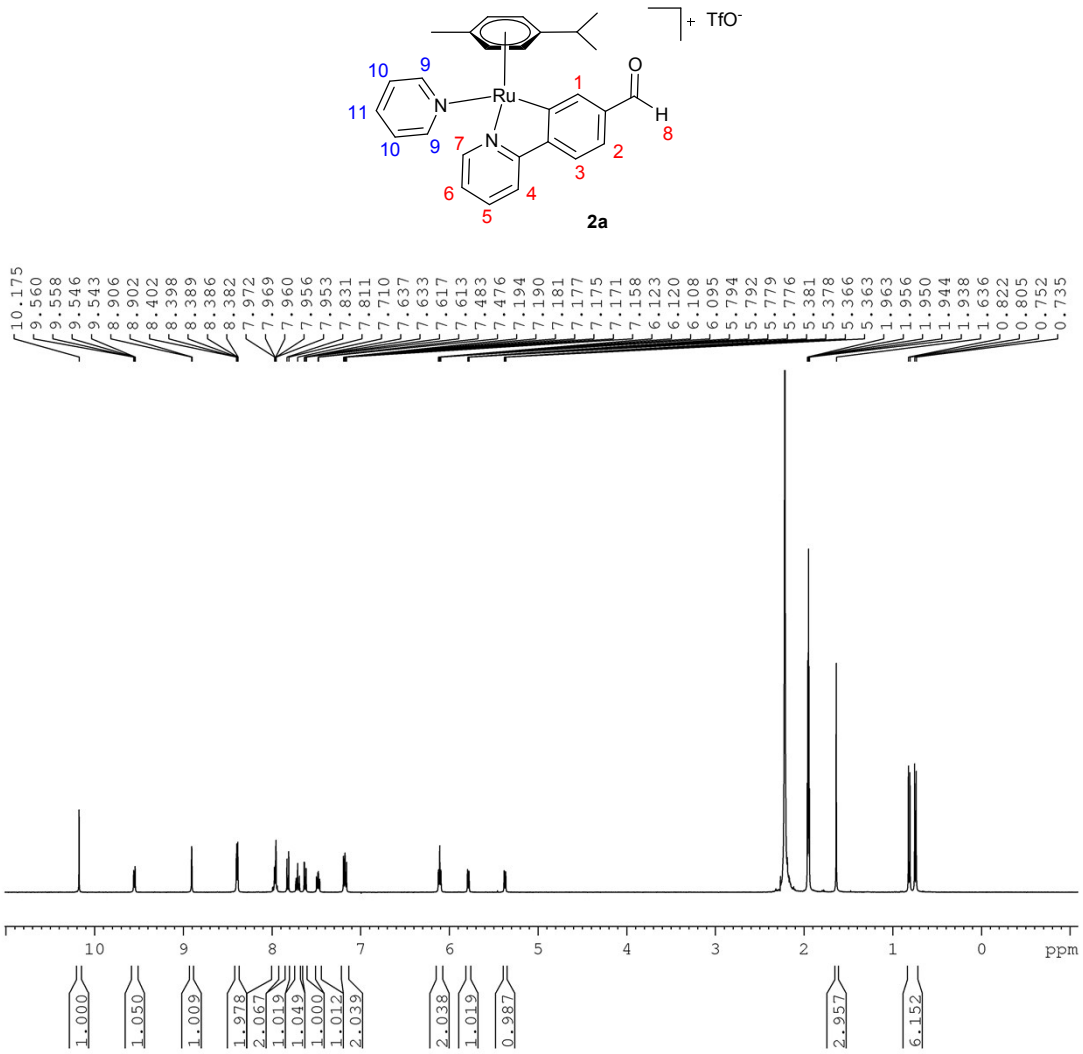

Figure S9. ^{1}H NMR spectrum of complex **2a** (in CD_3CN solution at 25 °C).

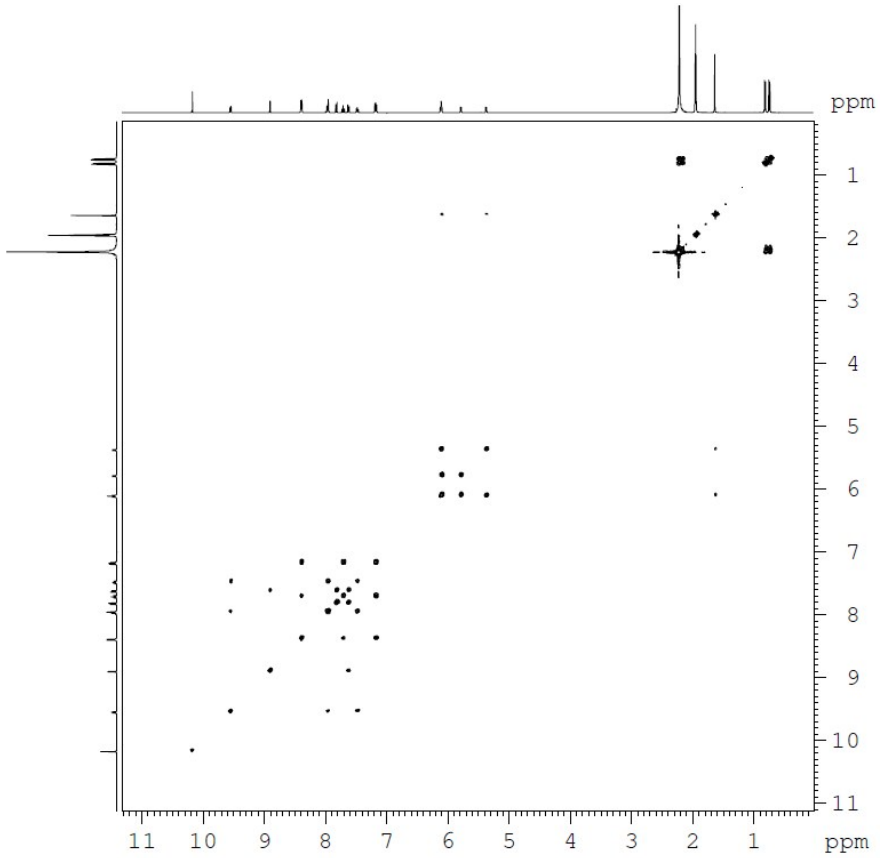

Figure S10. {^{1}H-^{1}H} COSY spectrum of complex **2a** (in CD_3CN solution at 25 °C).

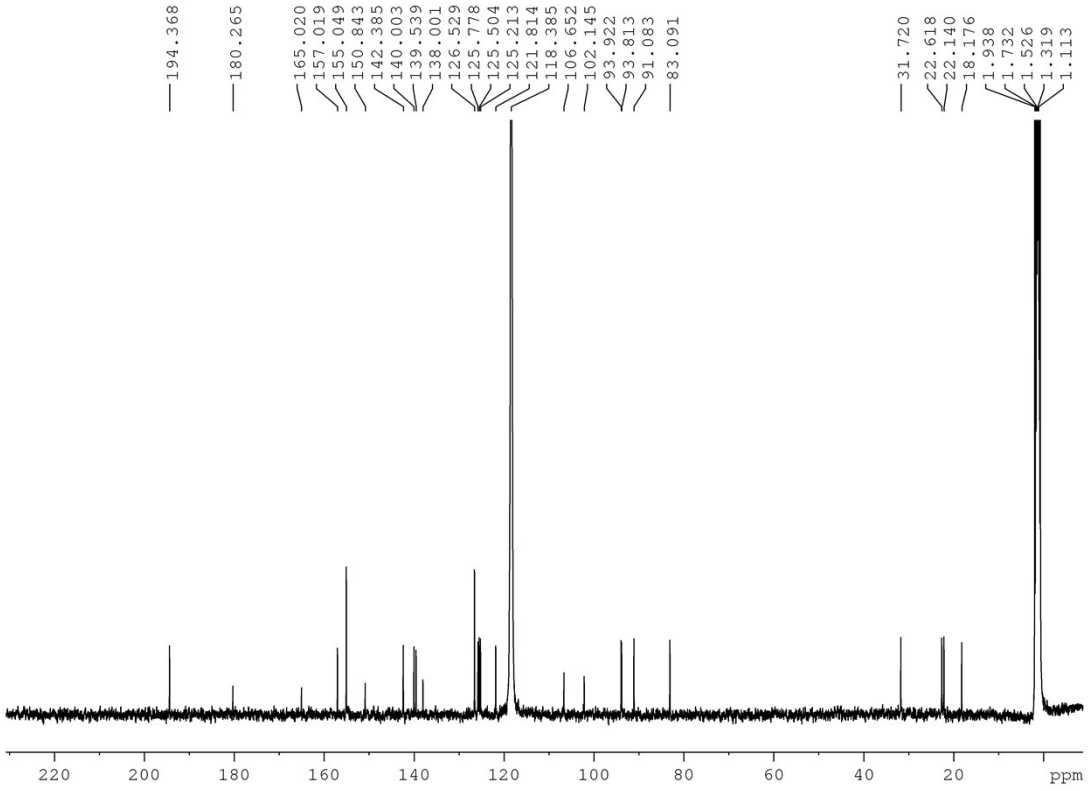

Figure S11. ^{13}C NMR spectrum of complex **2a** (in CD_3CN solution at 25 °C).

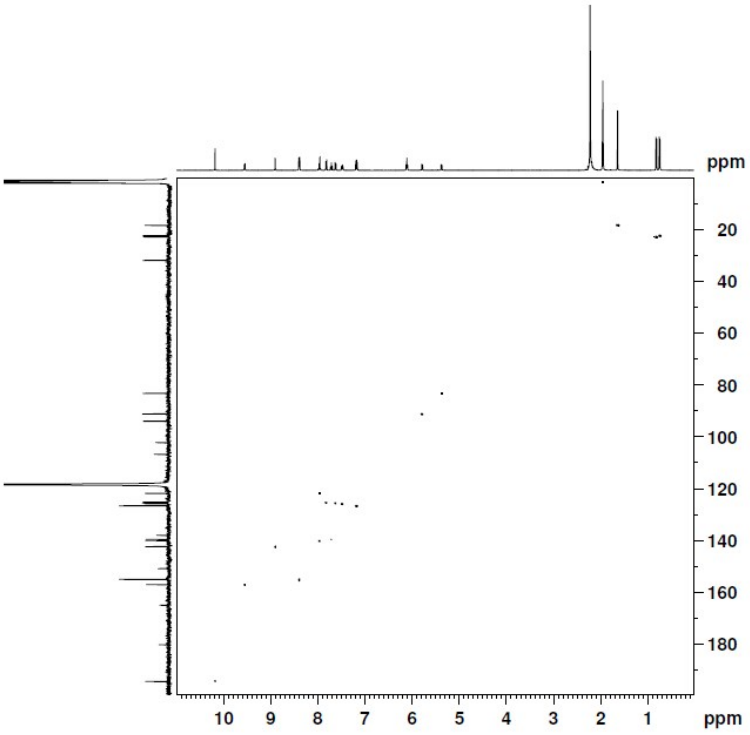

Figure S12. {^{1}H – ^{13}C} HSQC spectrum of complex **2a** (CD_3CN, 25 °C).

Compound 3a

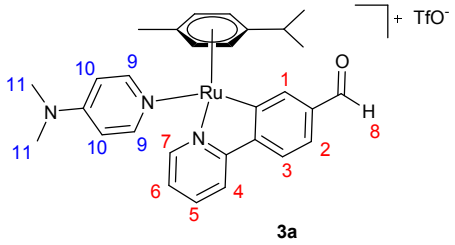

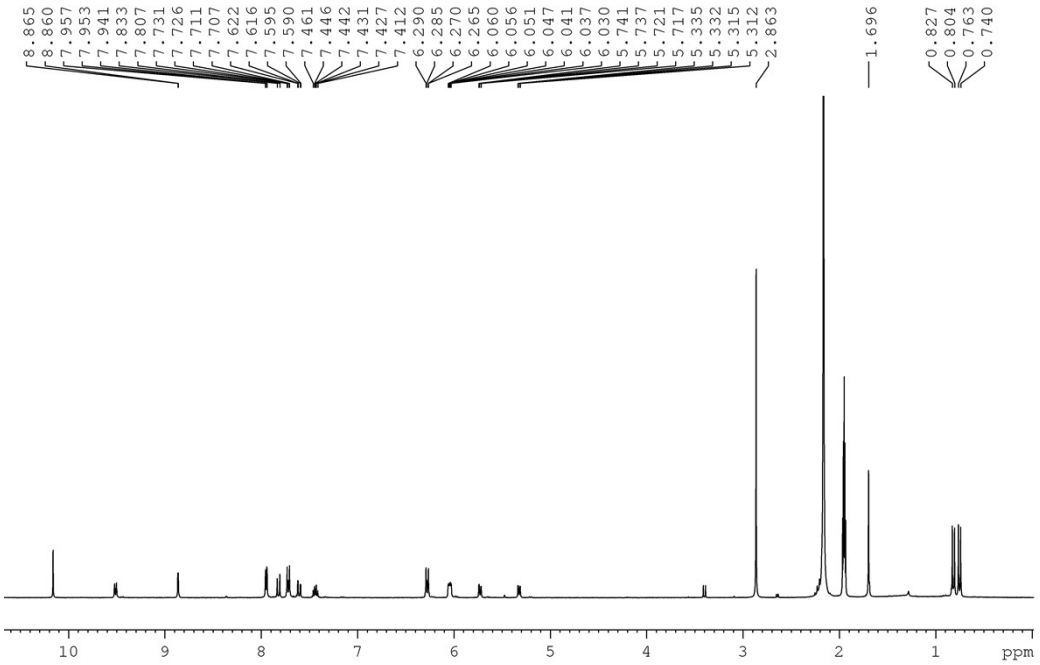

Figure S13. ^{1}H NMR spectrum of complex **3a** (in CD_3CN solution at 25 °C).

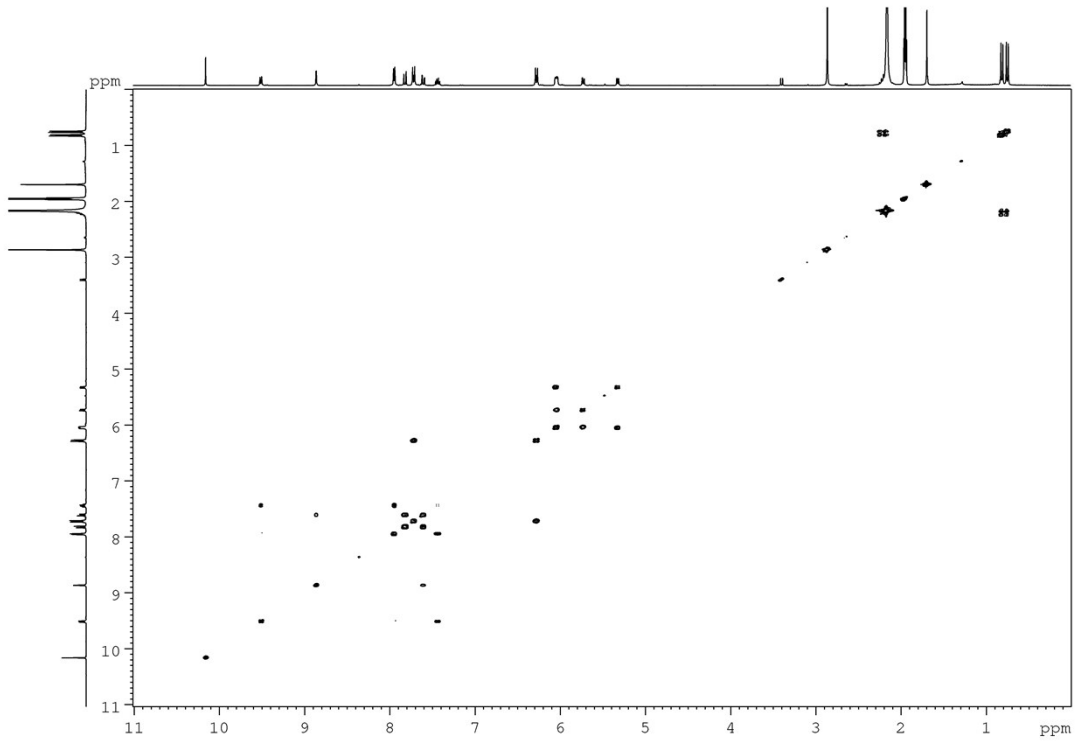

Figure S14. {^{1}H-^{1}H} COSY spectrum of complex **3a** (in CD_3CN solution at 25 °C).

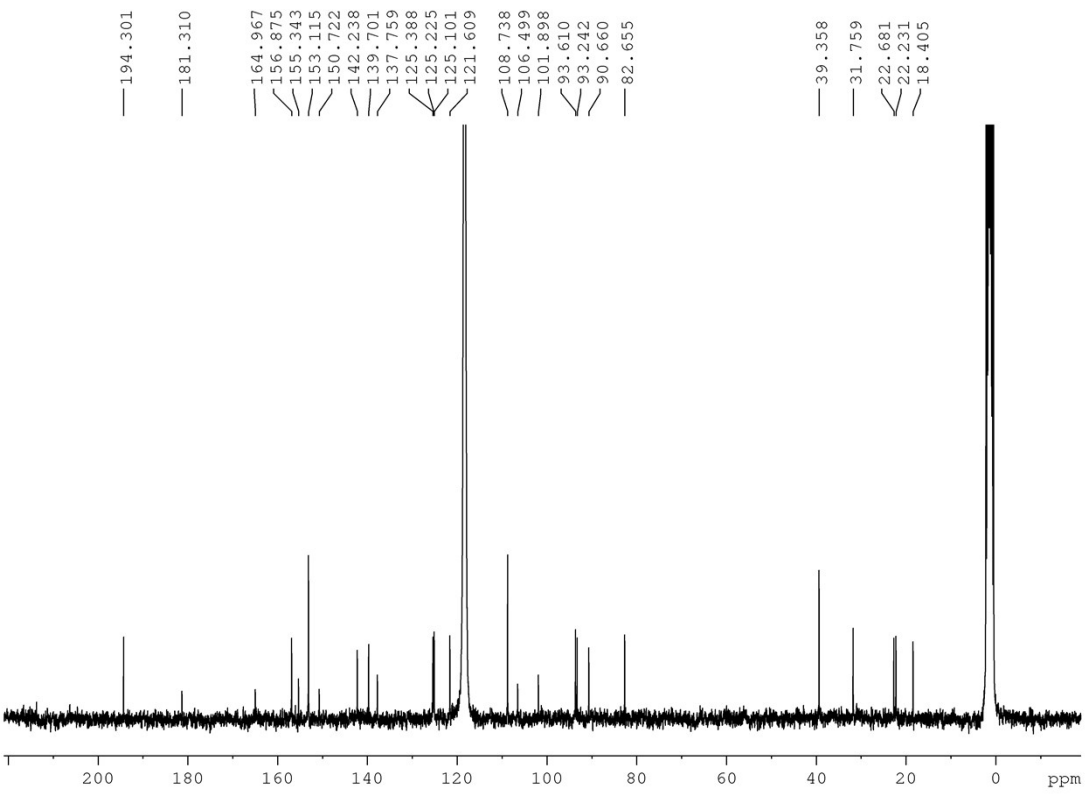

Figure S15. ^{13}C NMR spectrum of complex **3a** (in CD_3CN solution at 25 °C).

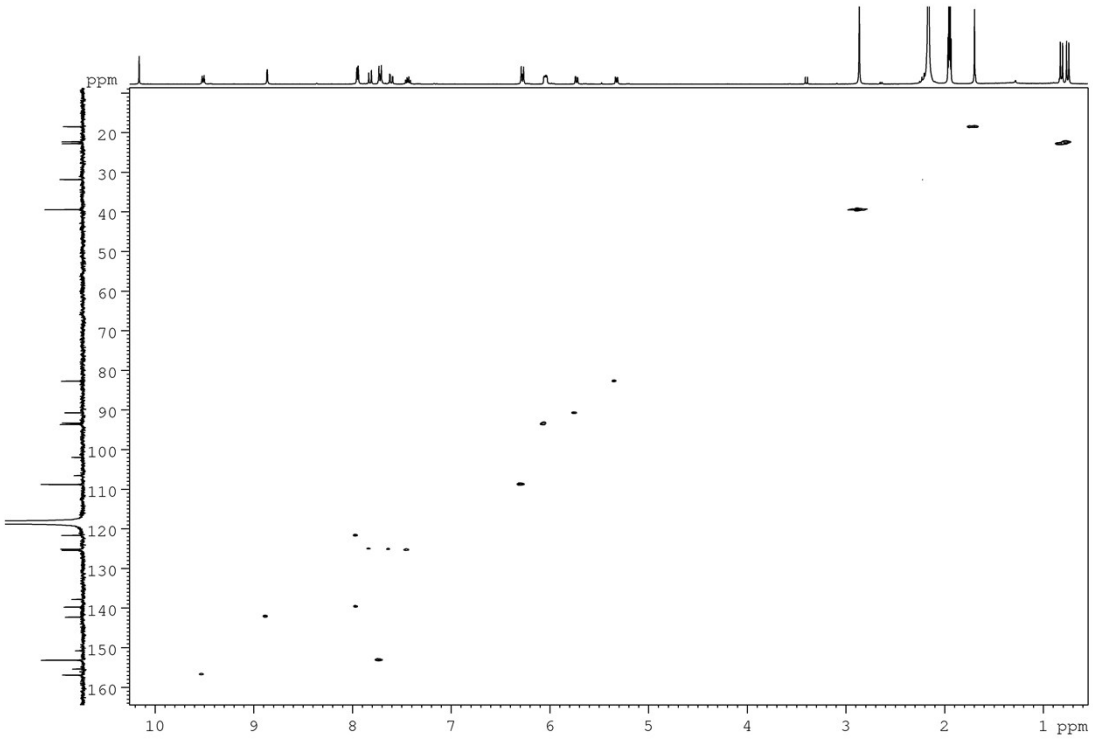

Figure S16. {^{1}H – ^{13}C} HSQC spectrum of complex **3a** (CD_3CN, 25 °C).

Compound 2b

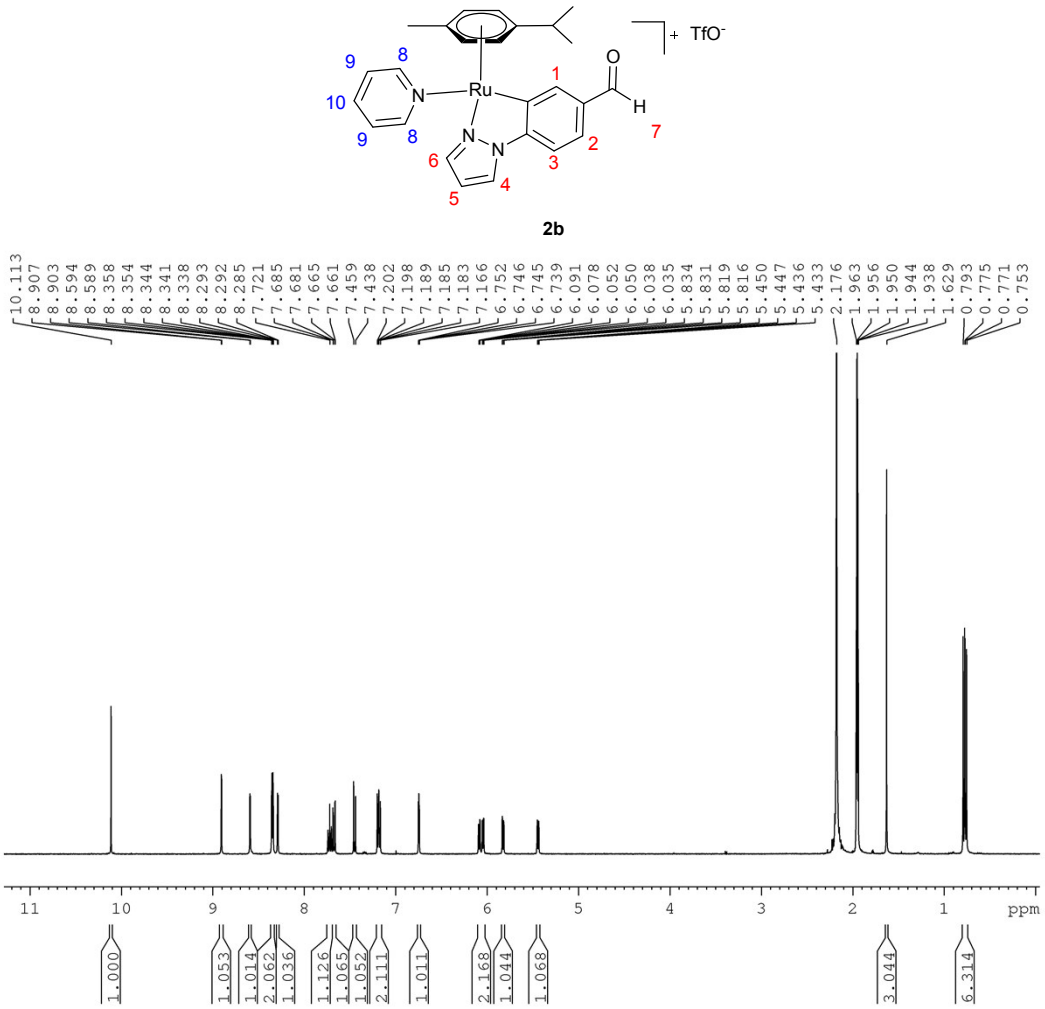

Figure S17. ^{1}H NMR spectrum of complex **2b** (in CD_3CN solution at 25 °C).

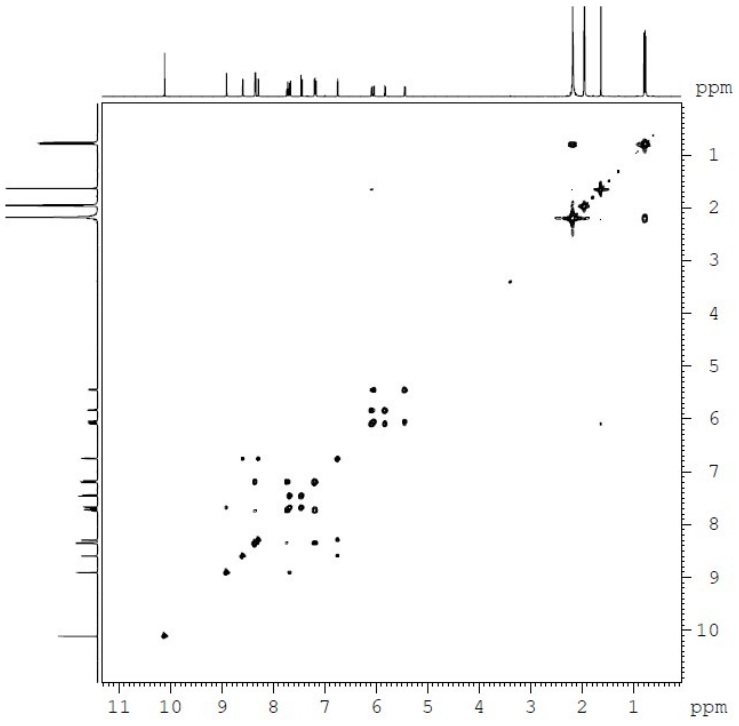

Figure S18. {^{1}H-^{1}H} COSY spectrum of complex **2b** (in CD_3CN solution at 25 °C).

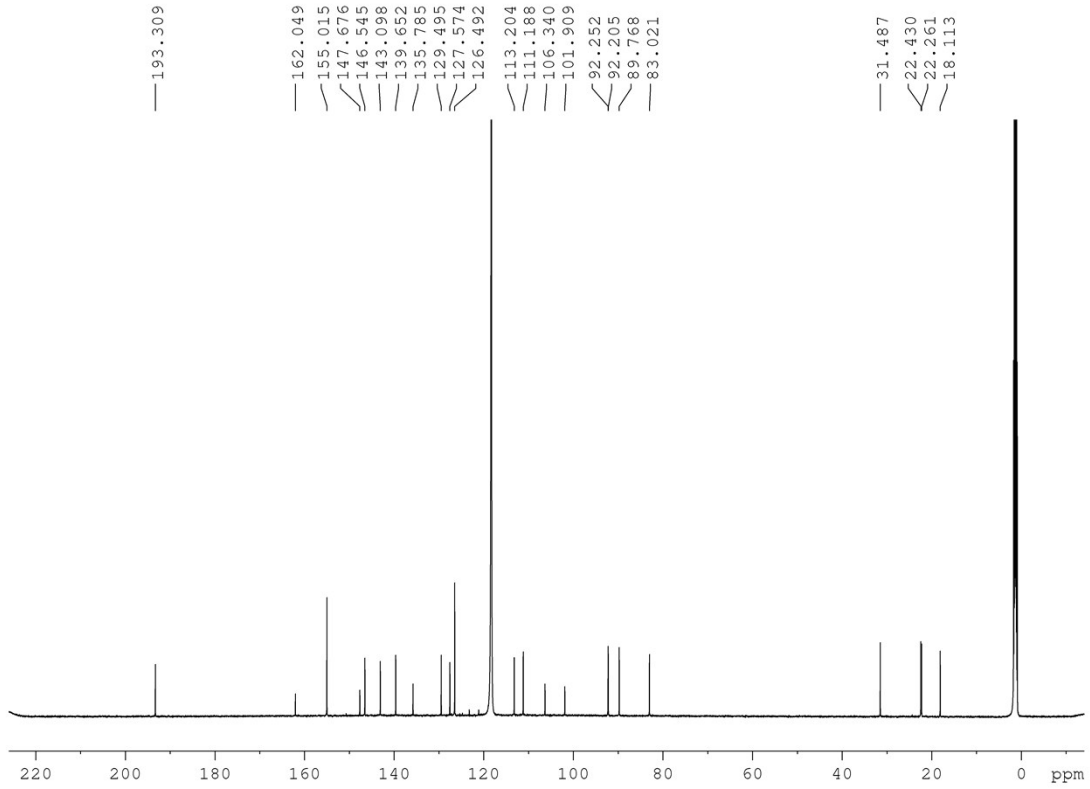

Figure S19. ^{13}C NMR spectrum of complex **2b** (in CD_3CN solution at 25 °C).

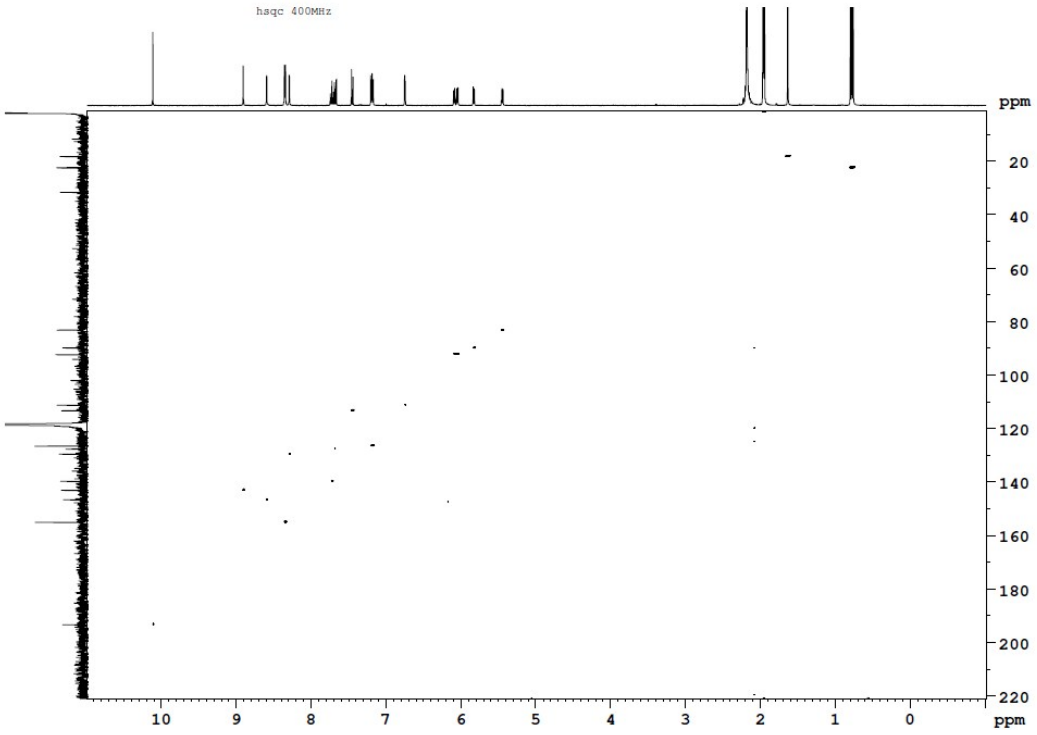

Figure S20. $\{^1H - ^{13}C\}$ HSQC spectrum of complex **2b** (CD_3CN, 25 °C).

Compound 3b

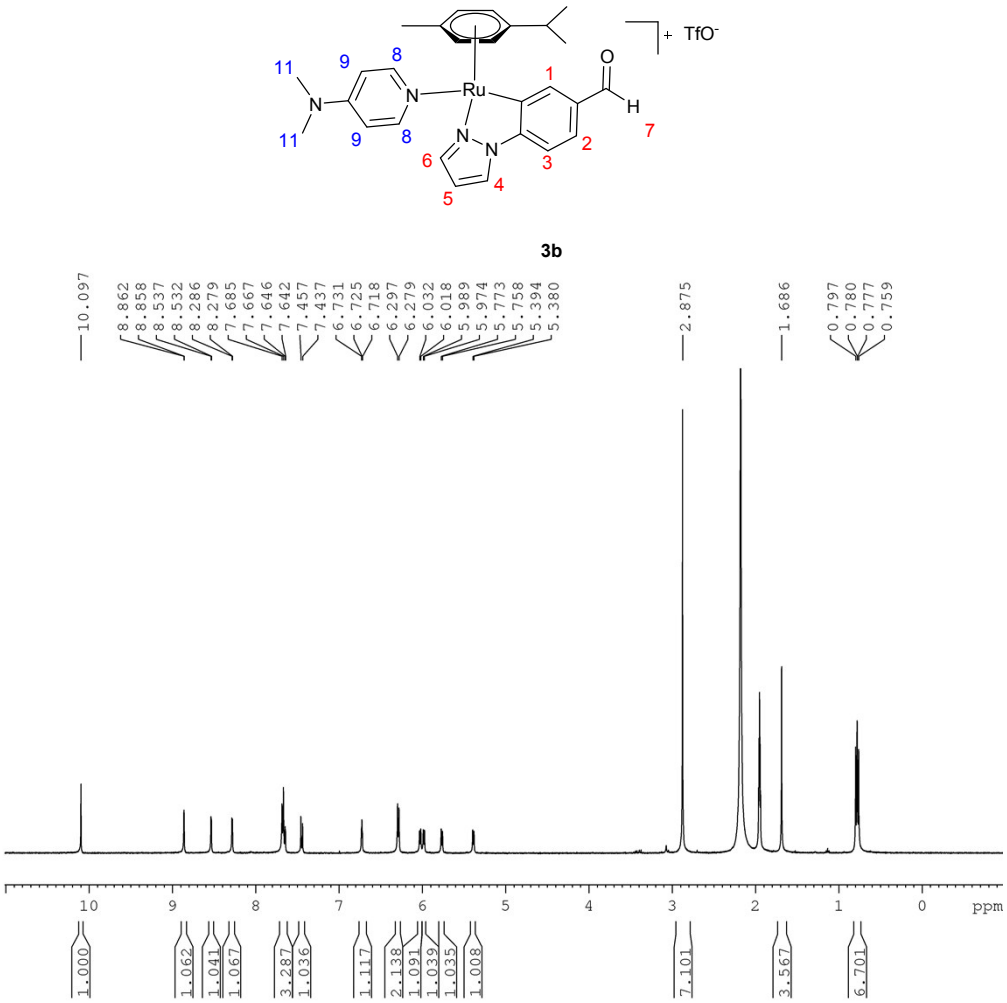

Figure S21. ^{1}H NMR spectrum of complex **3b** (in CD_3CN solution at 25 °C).

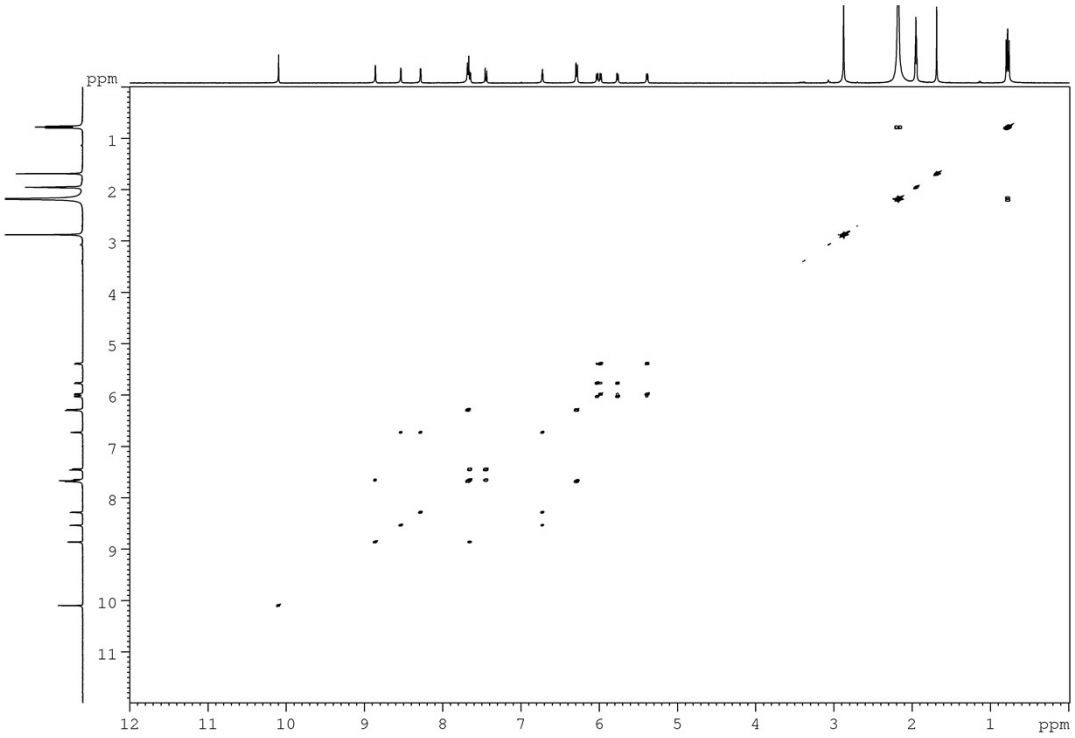

Figure S22. {^{1}H-^{1}H} COSY spectrum of complex **3b** (in CD_3CN solution at 25 °C).

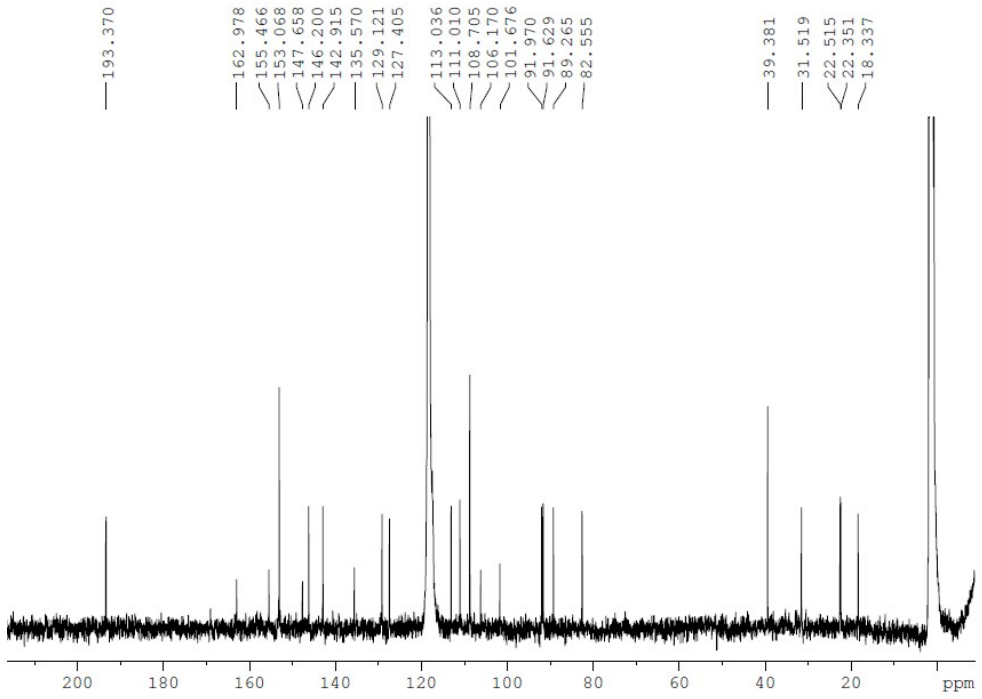

Figure S23. ^{13}C NMR spectrum of complex **3b** (in CD_3CN solution at 25 °C).

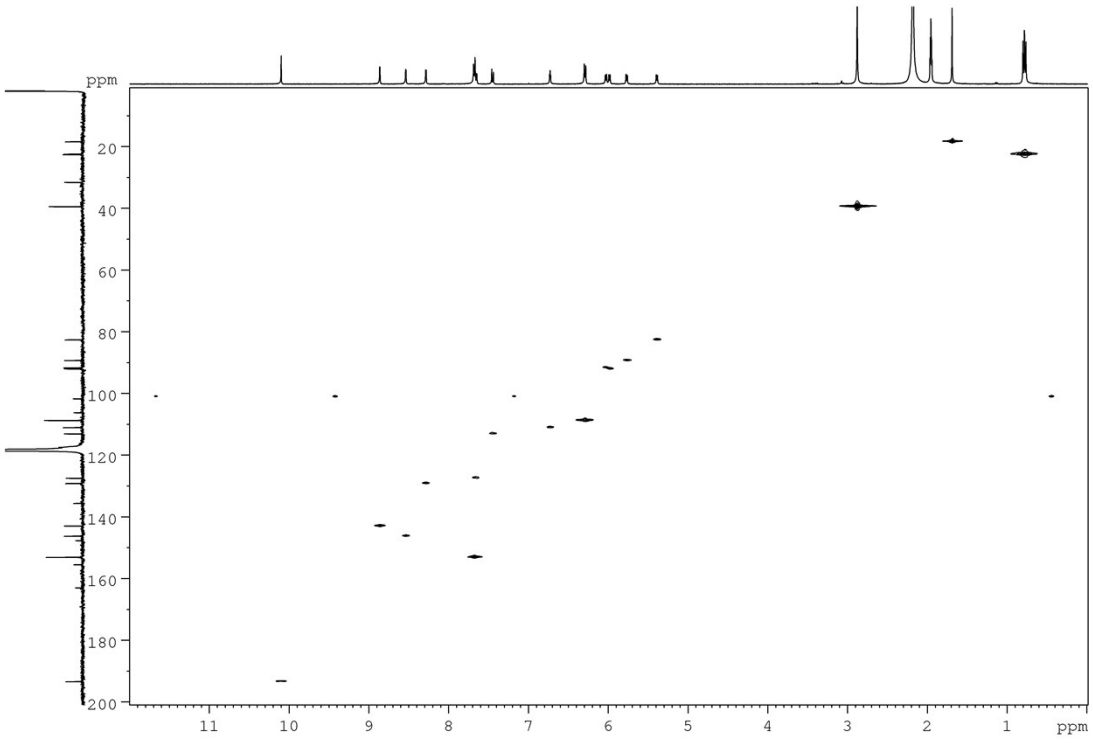

Figure S24. {^{1}H – ^{13}C} HSQC spectrum of complex **3b** (CD_3CN, 25 °C).

HPLC purity analyses

The purity of Ru(II) complexes was analyzed using a RP-HPLC/MS TOF 6220 equipped with a double binary pump (model G1312A), degasser, autosampler (model G1329A), diode array detector (model G1315D) and mass detector in series Agilent Technologies 1200. Chromatographic analyses were carried out on a Brisa C18 column (200 mm × 4.6 mm, 5 µm particle size). The mobile phase was a mixture of (A) H2O/HCOOH 0.1% and (B) acetonitrile/HCOOH 0.1%. The flow rate was 0.6 mL min−1 in a linear gradient starting with 10% B at 0–14 min, reaching 90% B at 14.1–18 min, and 10% B at 18.1–20 min. Chromatograms were recorded at 280 nm. The HPLC system was controlled by a ChemStation software (MASS HUNTER). Samples were dissolved in DMSO (1 mg mL-1 final concentration).

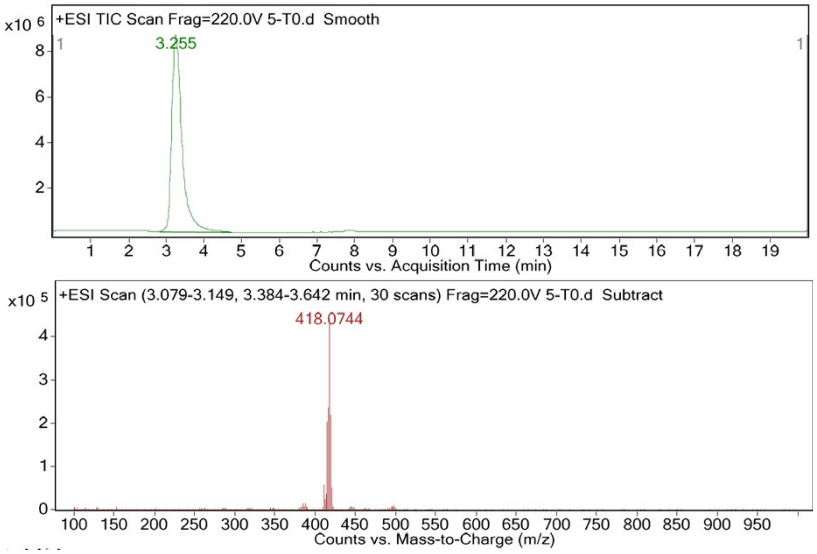

Figure S25. HPLC chromatograms of **2a** (ca. 50 µM) in DMSO t = 0 h (top). ESI-MS (pos ion mode) observed at T_R ~ 3.255 ($[M\text{-}X]^+$) of **2a** (bottom).

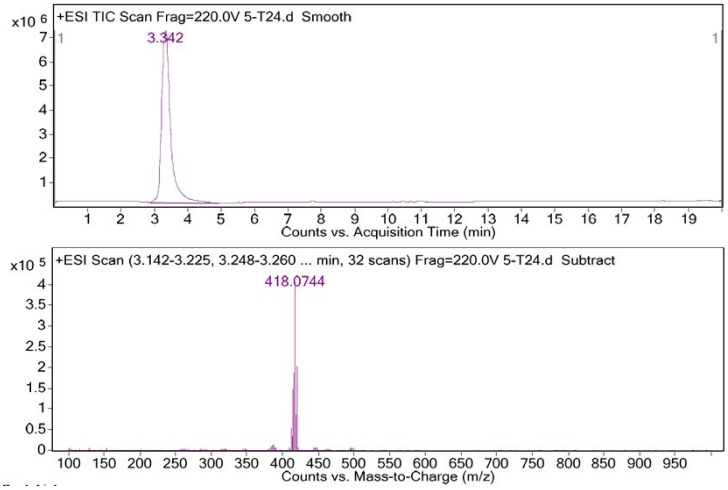

Figure S26. HPLC chromatograms of **2a** (ca. 50 µM) in DMSO t = 24 h (top). ESI-MS (pos ion mode) observed at T_R ~ 3.34 ($[M\text{-}X]^+$) of **2a** (bottom).

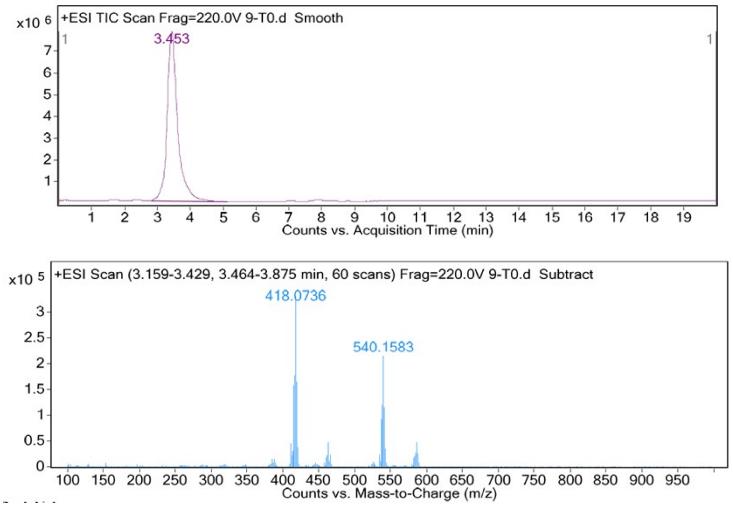

Figure S27. HPLC chromatograms of **3a** (ca. 50 µM) in DMSO t = 0 h (top). ESI-MS (pos ion mode) observed at T_R ~ 3.45 ($[M\text{-}X]^+$) of **3a** (bottom).

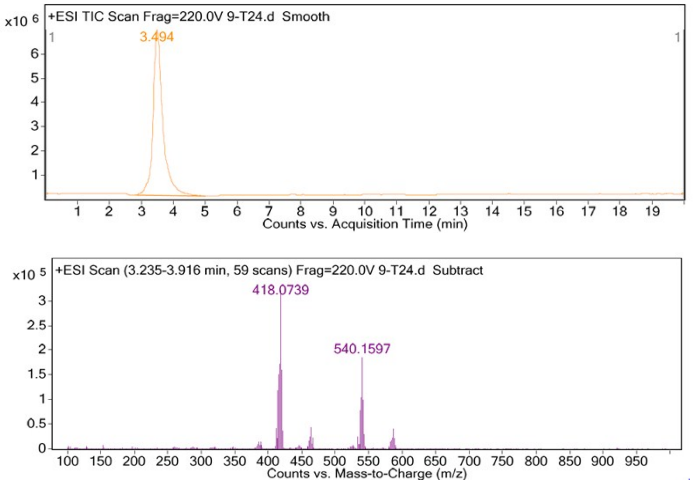

Figure S28. HPLC chromatograms of **3a** (ca. 50 µM) in DMSO t = 24 h (top). ESI-MS (pos ion mode) observed at T_R ~ 3.49 ($[M\text{-}X]^+$) of **3a** (bottom).

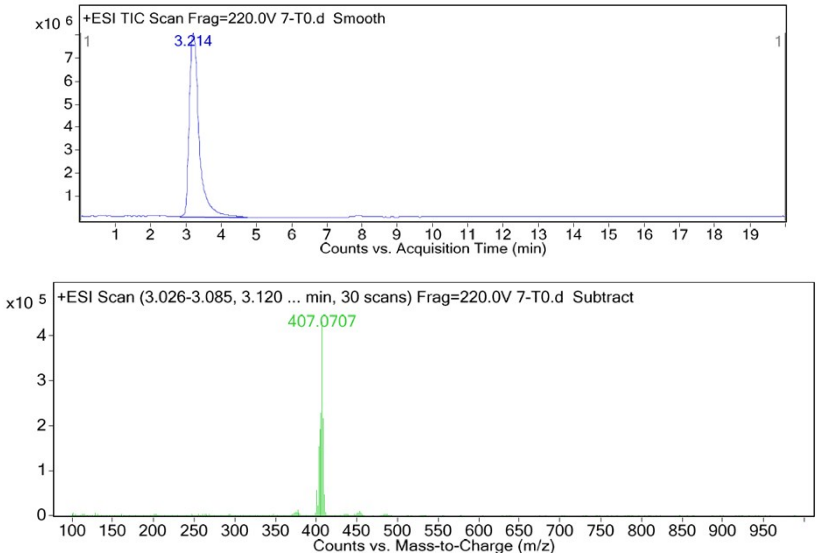

Figure S29. HPLC chromatograms of **2b** (ca. 50 µM) in DMSO t = 0 h (top). ESI-MS (pos ion mode) observed at T_R ~ 3.21 ($[M\text{-}X]^+$) of **2b** (bottom).

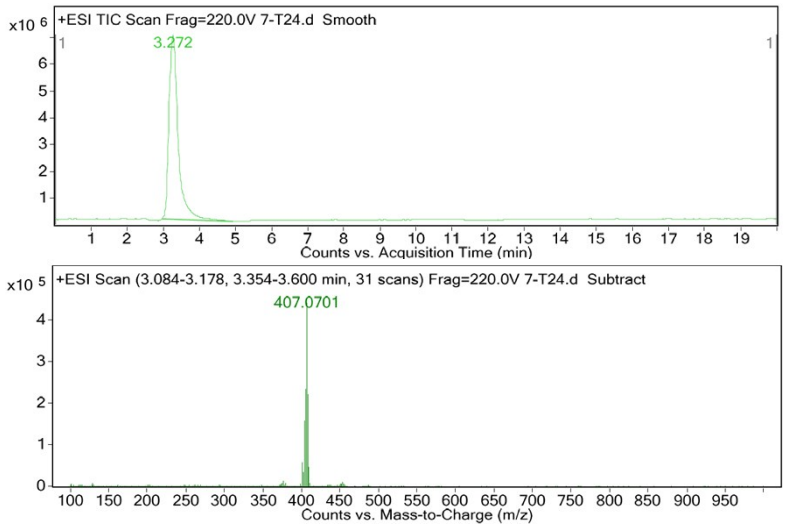

Figure S30. HPLC chromatograms of **2b** (ca. 50 μM) in DMSO t = 24 h (top). ESI-MS (pos ion mode) observed at T_R ~ 3.27 ($[M\text{-}X]^+$) of **2b** (bottom).

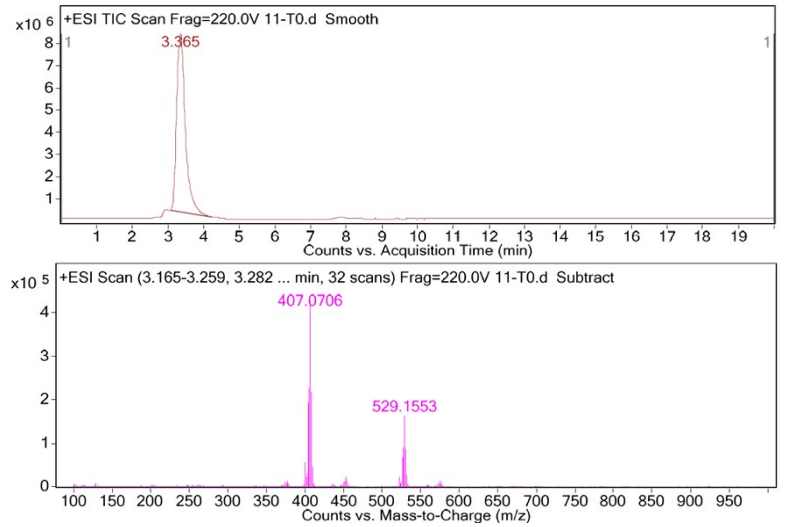

Figure S31. HPLC chromatograms of **3b** (ca. 50 μM) in DMSO t = 0 h (top). ESI-MS (pos ion mode) observed at T_R ~ 3.27 ($[M\text{-}X]^+$) of **3b** (bottom).

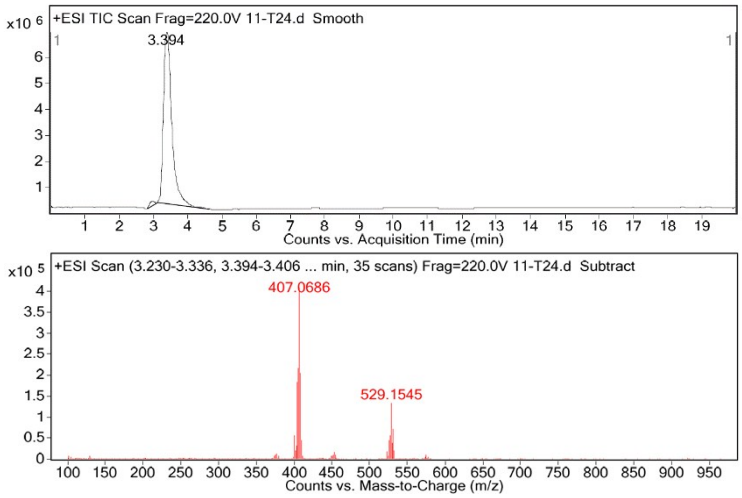

Figure S32. HPLC chromatograms of **3b** (ca. 50 µM) in DMSO t = 24 h (top). ESI-MS (pos ion mode) observed at T_R ~ 3.27 ($[M\text{-}X]^+$) of **3b** (bottom).

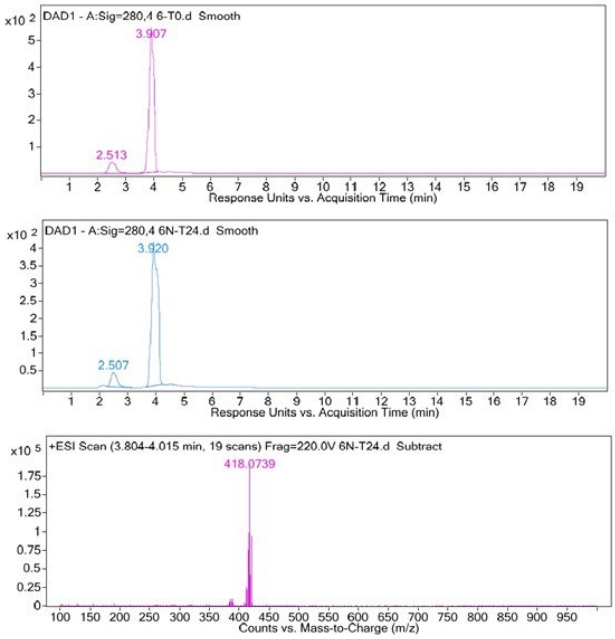

Figure S33. HPLC chromatograms of **2a** (ca. 50 µM) in RPMI culture medium (3% DMSO) at t = 0 h (top) and t = 24 h (middle) T_R ~ 2.5 (RPMI). ESI-MS (pos ion mode) observed at T_R ~ 3.9 ($[M^+\text{-py}]$) (bottom).

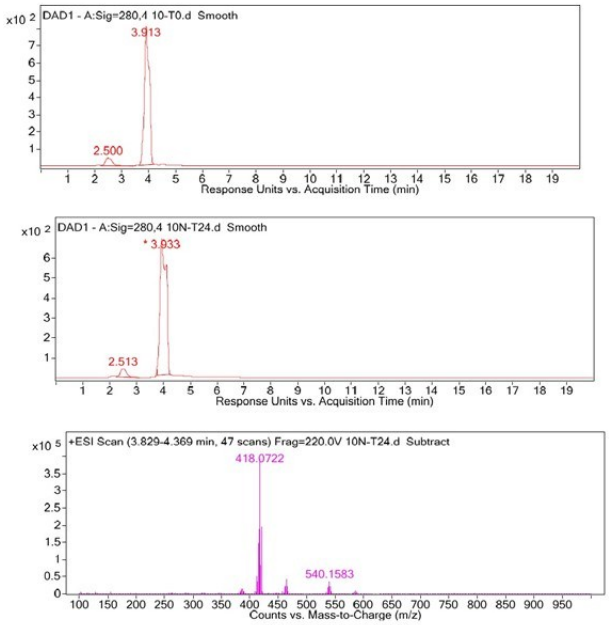

Figure S34. HPLC chromatograms of **3a** (ca. 50 μM) in RPMI culture medium (3% DMSO) at t = 0 h (top) and t = 24 h (middle) T_R ~ 2.5 (RPMI). ESI-MS (pos ion mode) observed at T_R ~ 3.9 ($[M]^+$; $[M^+\text{-}Me_2Npy]$) (bottom).

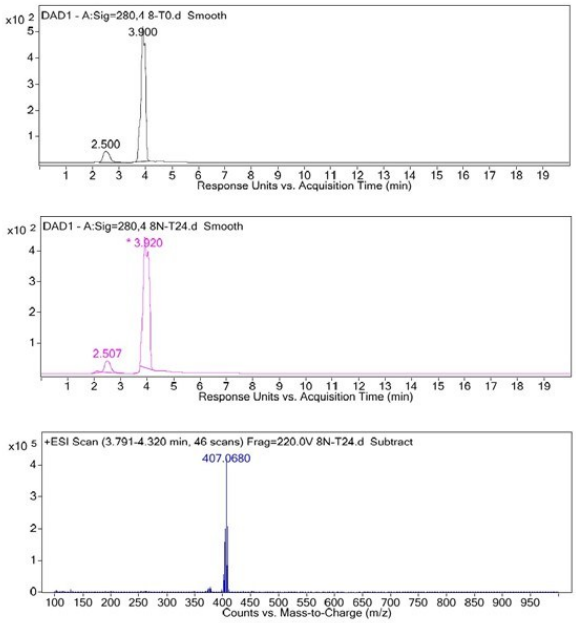

Figure S35. HPLC chromatograms of **2b** (ca. 50 μM) in RPMI culture medium (3% DMSO) at t = 0 h (top) and t = 24 h (middle) T_R ~ 2.5 (RPMI). ESI-MS (pos ion mode) observed at T_R ~ 3.9 ($[M^+\text{-}py]$) (bottom).

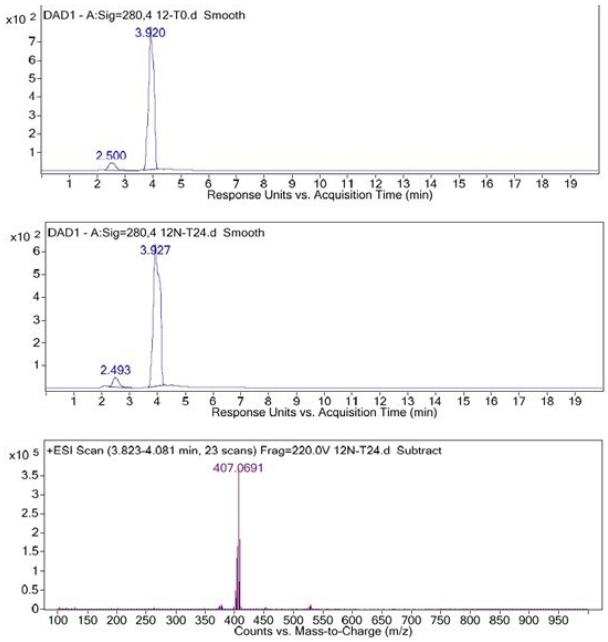

Figure S36. HPLC chromatograms of **3b** (ca. 50 μM) in RPMI culture medium (3% DMSO) at t = 0 h (top) and t = 24 h (middle) T_R ~ 2.5 (RPMI). ESI-MS (pos ion mode) observed at T_R ~ 3.9 ([M^+-NMe_2py]) (bottom).

Studies of interaction with oxidative biomolecules

The interaction of Ru(II) complexes **3a** and **3b** with oxidative biomolecules like N-acetyl-L-cysteine (L-NAC), glutathione reduced (GSH) and β-nicotinamide adenine dinucleotide (NADH) was studied by ^{1}H-NMR experiment in a Bruker AV 600 NMR spectrometer. Stock solutions of L-NAC, **3a** and **3b** were prepared in DMSO-d_6 and stock solutions of GSH and NADH were prepared in D_2O.

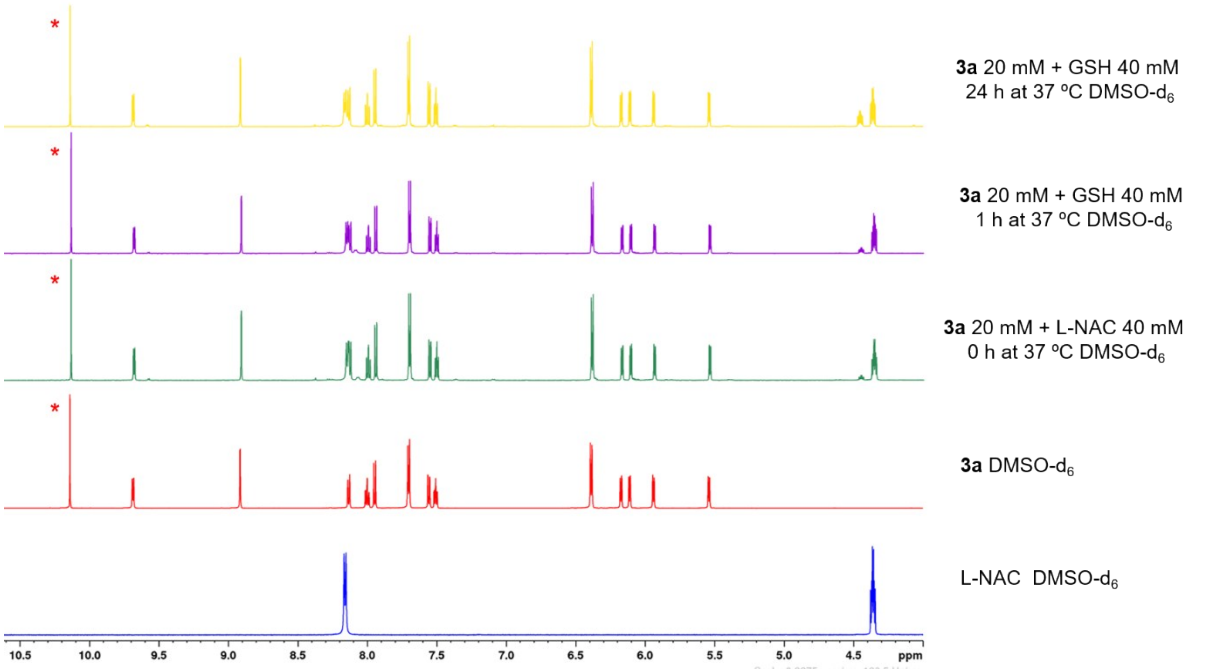

Figure S37. ^{1}H (600 MHz) NMR spectra of complex **3a** (20 mM) and L-NAC (40 mM) in 600 µL of DMSO-d_6. Peak about 10 ppm (*) correspond to proton of the aldehyde group.

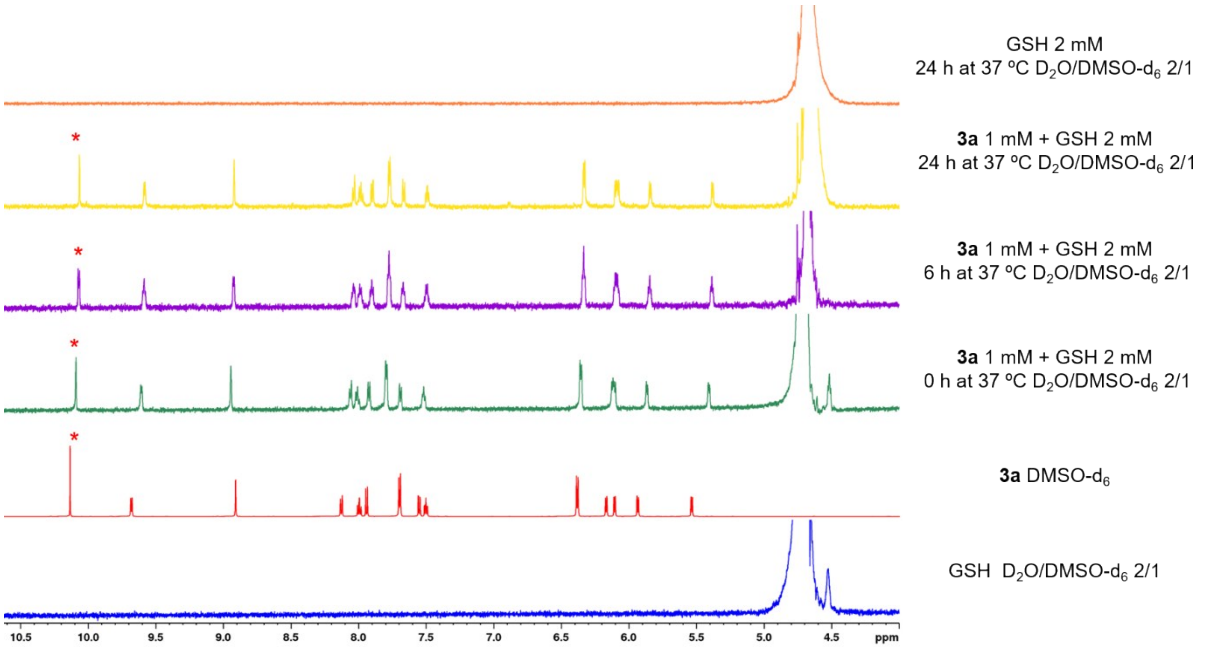

Figure S38. ^{1}H (600 MHz) NMR spectra of complex **3a** (1 mM) and GSH (2 mM) in 600 µL of a mixture 2/1 D_2O/DMSO-d_6. Peak about 10 ppm (*) correspond to proton of the aldehyde group.

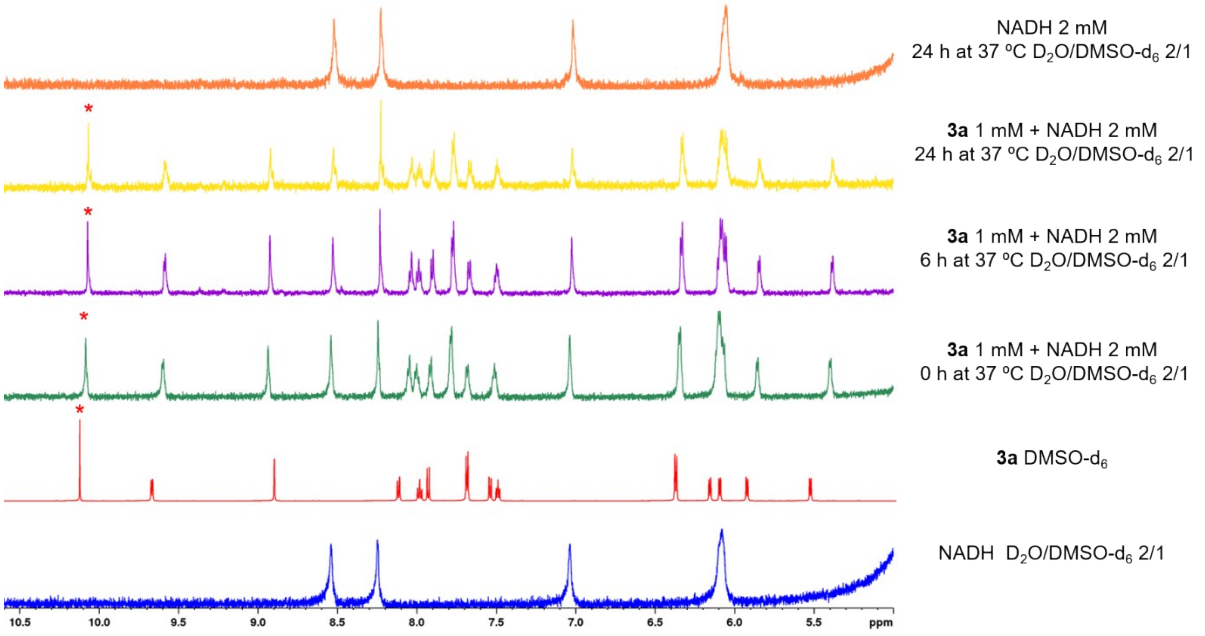

Figure S39. ^{1}H (600 MHz) NMR spectra of complex **3a** (1 mM) and NADH (2 mM) in 600 µL of a mixture 2/1 D_2O/DMSO-d_6. Peak about 10 ppm (*) correspond to proton of the aldehyde group.

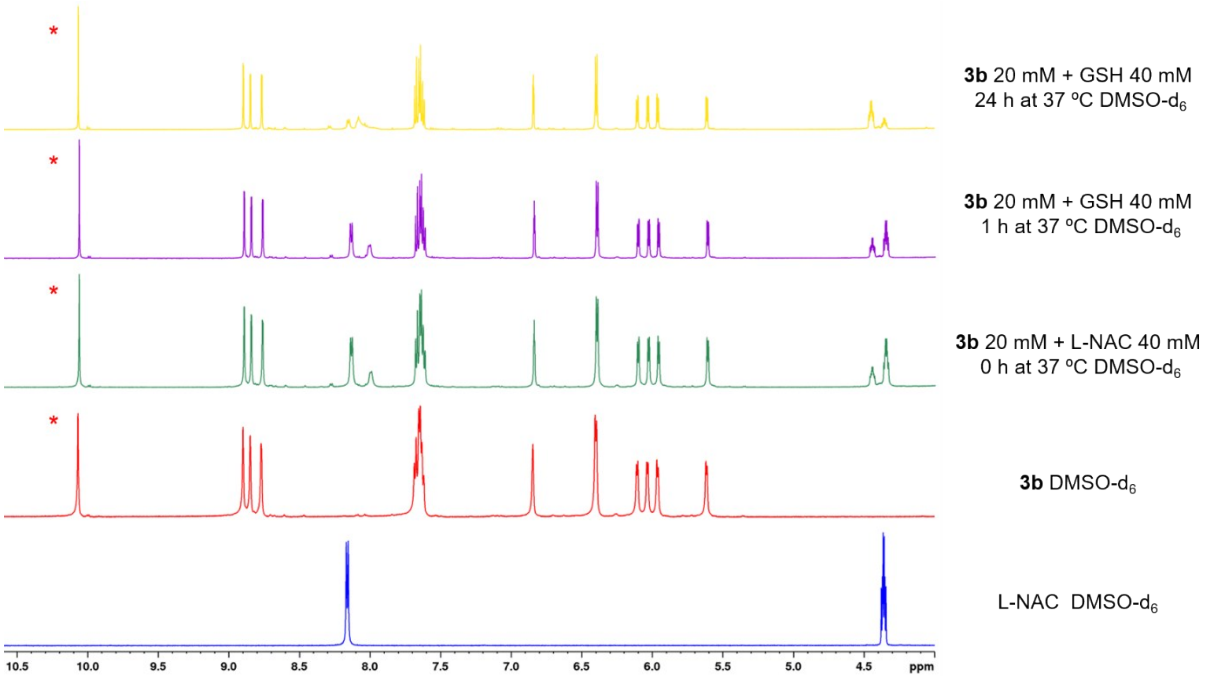

Figure S40. ^{1}H (600 MHz) NMR spectra of complex **3b** (20 mM) and L-NAC (40 mM) in 600 µL of DMSO-d_6. Peak about 10 ppm (*) correspond to proton of the aldehyde group.

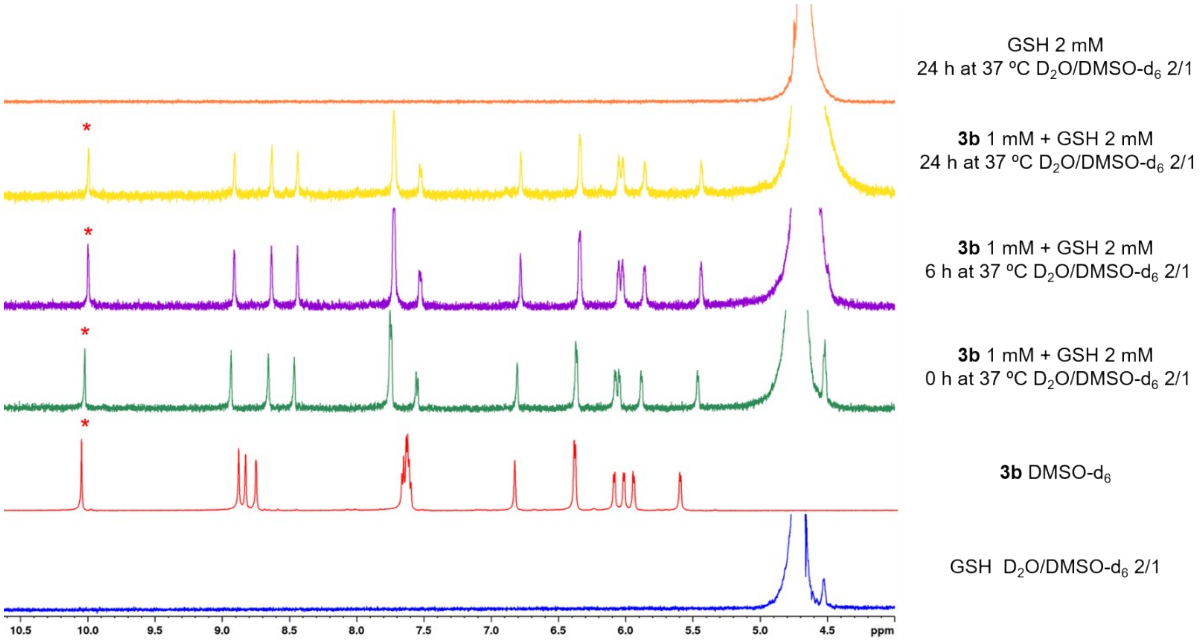

Figure S41. ^{1}H (600 MHz) NMR spectra of complex **3b** (1 mM) and GSH (2 mM) in 600 µL of a mixture 2/1 D_2O/DMSO-d_6. Peak about 10 ppm (*) correspond to proton of the aldehyde group.

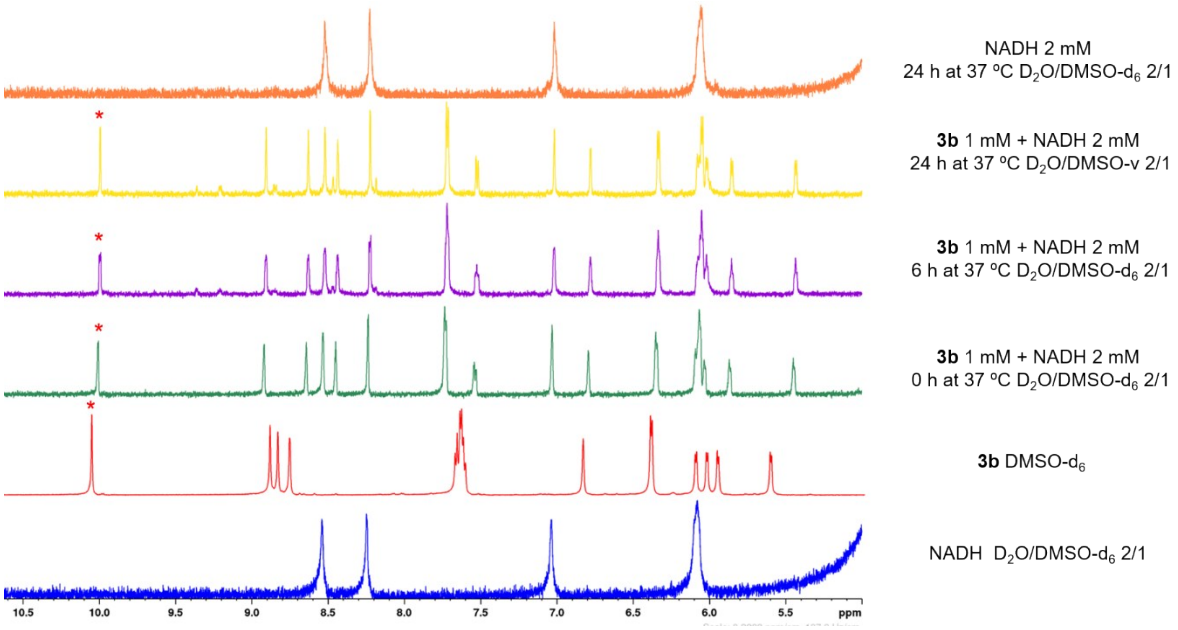

Figure S42. ^{1}H (600 MHz) NMR spectra of complex **3b** (1 mM) and NADH (2 mM) in 600 µL of a mixture 2/1 D_2O/DMSO-d_6. Peak about 10 ppm (*) correspond to proton of the aldehyde group.

Hydrolysis studies

Stock solutions of complexes **1a, 1b, 2a** and **3a** were prepared in MeOD-d_4 (3 mM), and the NaCl stock solution was prepared by solving in D_2O (0.5 M).

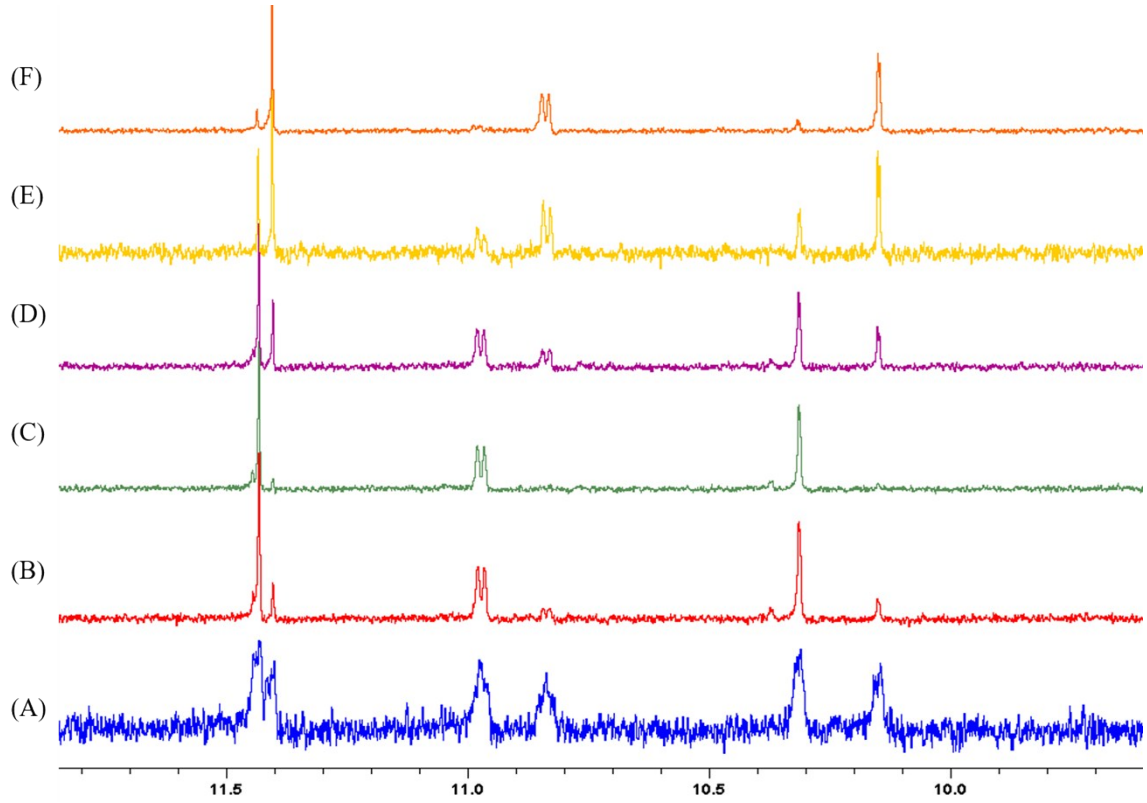

Figure S43. ^1H (400 MHz) NMR spectra of complex **1a** (1 mM) in 600 µL of 1/2 MeOD-d_4 / D_2O (v/v) (A) after 5 min; (B) after 15 min; (C) after 60 min; (D) Same sample with and addition of 4 mM of NaCl after 30min. (E) Same sample with and addition of 23 mM of NaCl after 30 min; (F) Spectra of a new sample of complex **1a** (1 mM) in 600 µL of 1/2 MeOD-d_4 / D_2O (v/v) with 100 mM of NaCl after 60 min.

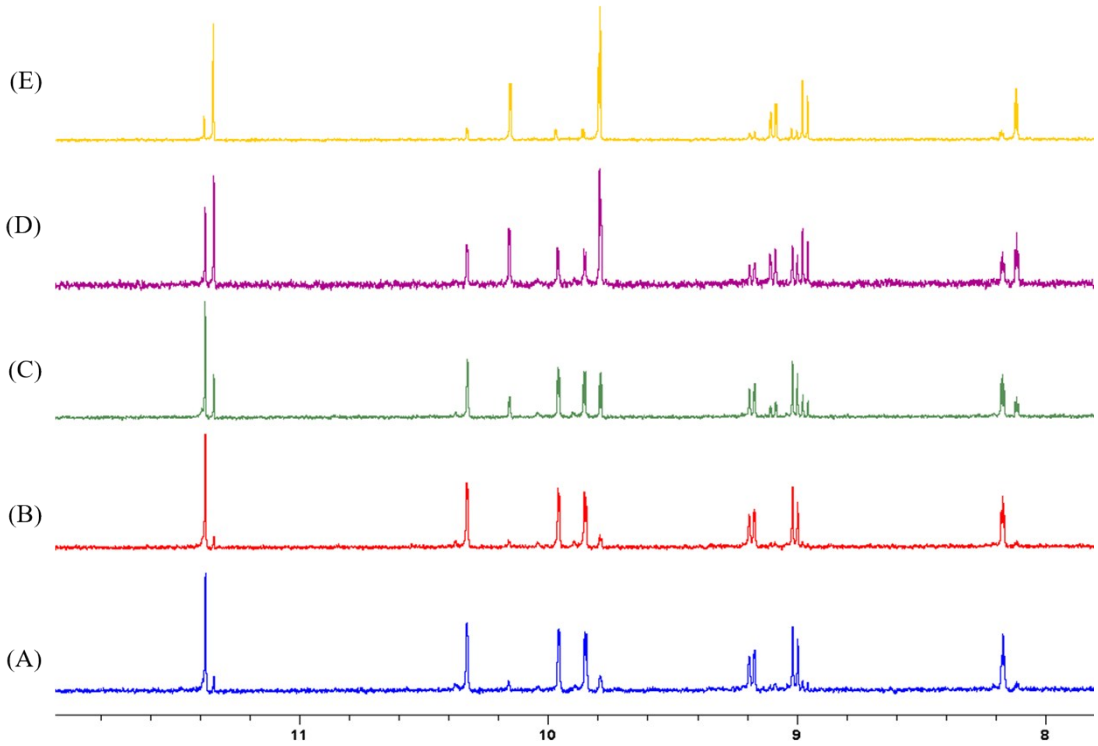

Figure S44. ^{1}H (400 MHz) NMR spectra of complex **1b** (1 mM) in 600 µL of 1/2 MeOD-d_4 / D_2O (v/v) (A) after 5 min; (B) after 30 min; (C) Same sample with and addition of 4 mM of NaCl after 30 min. (D) Same sample with and addition of 23 mM of NaCl after 30 min; (E) Spectra of a new sample of complex **1b** (1 mM) in 600 µL of 1/2 MeOD-d_4 / D_2O (v/v) with 100 mM of NaCl after 60 min.

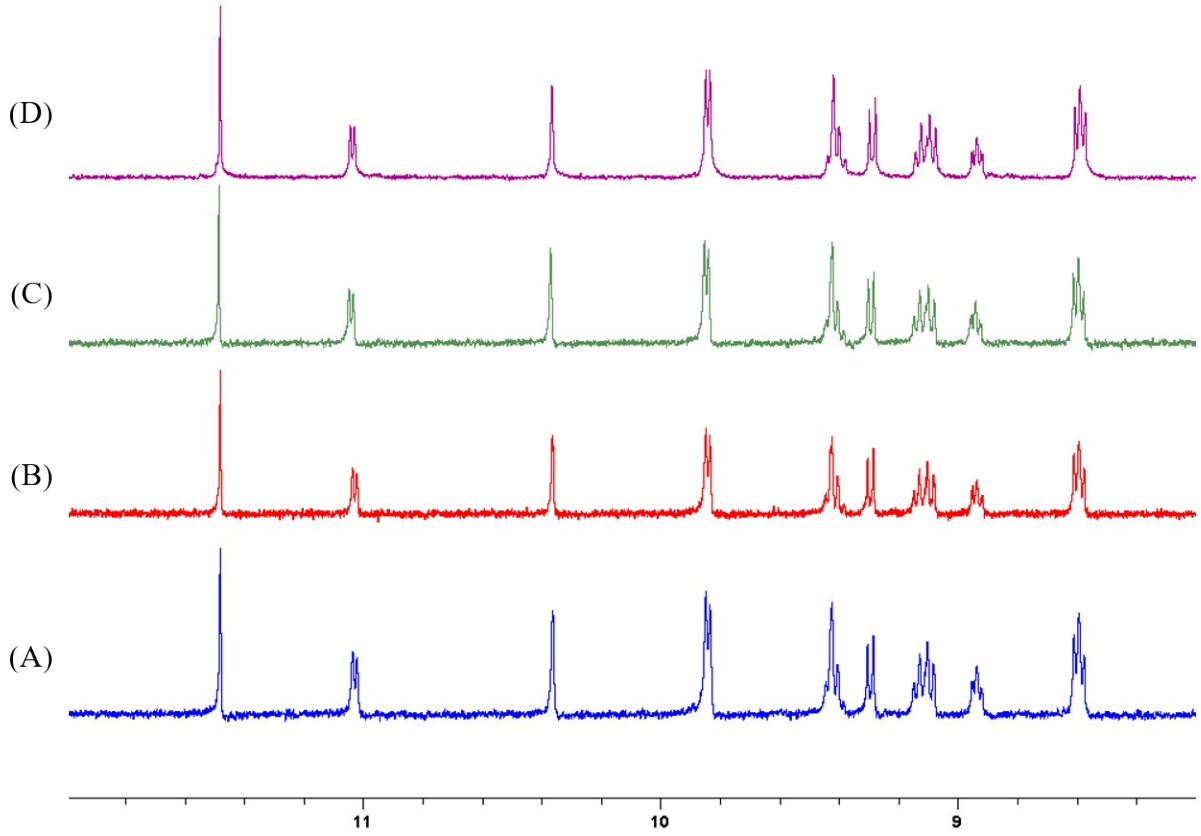

Figure S45. ^{1}H (400 MHz) NMR spectra of complex **2a** (1 mM) in 600 µL of 1/2 MeOD-d_4 / D_2O (v/v) (A) after 5 min; (B) after 60 min; (C) Spectra of a new sample of complex **2a** (1 mM) in 600 µL of 1/2 MeOD-d_4 / D_2O (v/v) with 100 mM of NaCl after 60 min; (D) after 9 days.

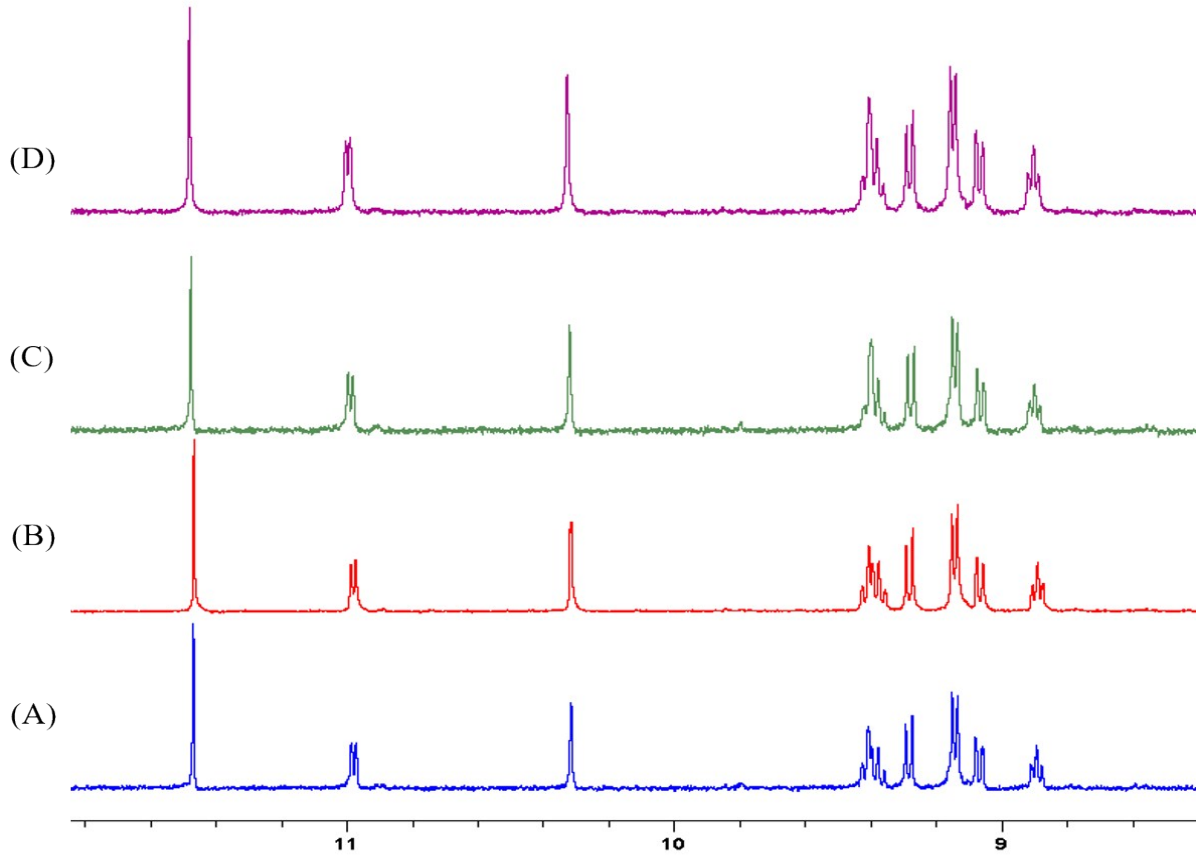

Figure S46. ^{1}H (400 MHz) NMR spectra of complex **3a** (1 mM) in 600 µL of 1/2 MeOD-d_4 / D_2O (v/v) (A) after 5 min; (B) after 60 min; (C) Spectra of a new sample of complex **3a** (1 mM) in 600 µL of 1/2 MeOD-d_4 / D_2O (v/v) with 100 mM of NaCl after 60 min; (D) after 9 days.

X-ray Crystallographic Analysis

Crystals suitable for X-ray diffraction of **1a, 1b, 2a** and **3a** were were obtained for complexes from acetonitrile / hexane (1:6) and mounted in inert oil on a glass fiber and transferred to the diffractometer. Intensities were registered at low temperature on a Bruker D8QUEST diffractometer using monochromated Mo Kα radiation (λ = 0.71073Å). Absorption corrections were based on multi-scans (program SADABS[1]). All non-hydrogen positions were refined with anisotropic temperature factors. Structures were refined anisotropically using SHELXL-2018.[2] Hydrogen atoms were included using rigid methyl groups or a riding model. A summary of crystal data collection and refinement parameters for all compounds are given in Tables S1-S8. Special features: for **2a** the triflate anion is disordered over two positions, ca. 51:49. The CHO and the methyl group are also disordered over two positions, ca. 52%:48% and 70%:30%, respectively.

Table S1. Crystal data and structure refinement for **1a, 1b, 2a** and **3a**				
Identification code	**1a**	**1b**	**2a**	**3a**
Empirical formula	$C_{22}H_{22}ClNORu$	$C_{20}H_{21}ClN_2ORu$	$C_{28}H_{27}F_3N_2O_4RuS$	$C_{30}H_{32}F_3N_3O_4RuS$
Formula weight	452.92	441.91	645.64	688.71
Temperature/ K	100(2)	100(2)	100(2)	100(2)
Wavelength/ Å	0.71073	0.71073	0.71073	0.71073
Crystal system	Monoclinic	Monoclinic	Monoclinic	Monoclinic
Space group	$P2_1/n$	$P2_1/n$	$P2_1/n$	$P2_1/n$
Unit cell dimensions				
a / Å	11.1703(6)	10.7146(5)	12.1052(16)	11.4821(7)
b / Å	13.1012(6)	13.1262(6)	16.953(2)	14.3856(8)
c / Å	12.5663(6)	12.7262(5)	12.9887(17)	17.8111(11)
α / °	90	90	90	90
β / °	90.3829(17)	92.545(2)	92.587(5)	96.525(2)
γ / °	90	90	90	90
Volume/ $Å^3$	1838.97(16)	1788.07(14)	2662.8(6) $Å^3$	2922.9(3)
Z	4	4	4	4
$Density_{calculated}$ / mg/m^3	1.636	1.642	1.611	1.565
Absorption coefficient / mm^{-1}	1.009	1.036	0.726	0.668
F(000)	920	896	1312	1408
Crystal size / mm^3	0. 450 x 0.140 x 0.090	0.266 x 0.230 x 0.100	0.250 x 0.150 x 0.011	0.210 x 0.120 x 0.050
Theta range / °	2.246 to 30.604	2.230 to 30.622	1.976 to 30.626	1.824 to 28.282
Index ranges	-15<=h<=15 -17<=k<=18 -17<=l<=18	-15<=h<=15 -18<=k<=18 -18<=l<=18	-17<=h<=17, -24<=k<=24 -18<=l<=18	-15<=h<=15 -19<=k<=19 -23<=l<=23
Reflections collected	60483	140718	292047	286523
Independent reflections	5647 R_{int} = 0.0342	5503 R_{int} = 0.0410	8194 R_{int} = 0.0491	7260 R_{int} = 0.0509
Completeness to theta = 25.242°	100.0 %	100.0 %	100.0 %	100.0 %
Absorption correction	Semi-empirical from equivalents	Semi-empirical from equivalents	Semi-empirical from equivalents	Semi-empirical from equivalents
Max. and min. transmission	0.8622 and 0.7756	0.7461 and 0.6845	0.7456 and 0.7132	0.7461 and 0.6985
Refinement method	Full-matrix least-squares on F^2	Full-matrix least-squares on F^2	Full-matrix least-squares on F^2	Full-matrix least-squares on F^2
Data / restraints / parameters	5647 / 0 / 238	5503 / 0 / 229	8194 / 168 / 458	7260 / 0 / 384
Goodness-of-fit on F^2	1.079	1.084	1.132	1.106
Final R indices [I>2sigma(I)]	R1 = 0.0209 wR2 = 0.0473	R1 = 0.0219 wR2 = 0.0475	R1 = 0.0281 wR2 = 0.0607	R1 = 0.0277 wR2 = 0.0617
R indices (all data)	R1 = 0.0263 wR2 = 0.0489	R1 = 0.0274 wR2 = 0.0494	R1 = 0.0311 wR2 = 0.0617	R1 = 0.0327 wR2 = 0.0635
Largest diff. peak and hole / $e.Å^{-3}$	0.541 and -0.669	0.479 and -0.818	0.447 and -0.534	1.477 and -0.536

Table S2. Bond lengths [Å] and angles [°] for complexes **1a, 1b, 2a** and **3a**				
	1a	**1b**	**2a**	**3a**
Ru1Cl1	2.4287(5)	2.4276(5)		

Ru1N1	2.093(1)	2.066(1)	2.082(1)	2.079(1)
Ru1C1	2.191(1)	2.184(1)	2.193(2)	2.210(2)
Ru1C2	2.171(1)	2.247(1)	2.264(2)	2.186(2)
Ru1C3	2.197(1)	2.267(1)	2.283(2)	2.204(2)
Ru1C4	2.241(1)	2.235(1)	2.226(3)	2.235(2)
Ru1C5	2.286(1)	2.194(1)	2.193(2)	2.276(2)
Ru1C6	2.279(1)	2.162(1)	2.169(2)	2.196(2)
Ru1C11	2.041(1)	2.053(1)	2.047(2)	2.044(2)
Ru1 N31			2.114(1)	
Ru1 N23				2.122(1)
Cl1Ru1N1	87.02(3)	87.79(3)		
Cl1Ru1C1	154.69(4)	157.68(4)		
Cl1Ru1C2	157.35(4)	120.05(4)		
Cl1Ru1C3	119.27(4)	94.54(4)		
Cl1Ru1C4	93.21(4)	92.07(4)		
Cl1Ru1C5	93.75(4)	116.80(4)		
Cl1Ru1C6	117.75(4)	154.81(4)		
Cl1Ru1C11	86.53(4)	86.56(4)		
N1Ru1C1	91.49(5)	91.20(5)	92.94(6)	104.65(6)
N1Ru1C2	115.01(5)	94.85(5)	95.88(7)	137.57(6)
N1Ru1C3	152.51(5)	121.13(5)	121.14(7)	171.62(6)
N1Ru1C4	161.13(5)	158.24(5)	157.61(7)	139.52(6)
N1Ru1C5	124.26(5)	154.55(5)	156.35(7)	107.60(6)
N1Ru C6	97.44(5)	116.47(5)	118.15(6)	92.59(6)
N1Ru1C11	77.97(5)	77.40(5	78.10(6)	78.10(7)
N1Ru1N31			87.00(5)	
N1 Ru1 N23				84.77(6)

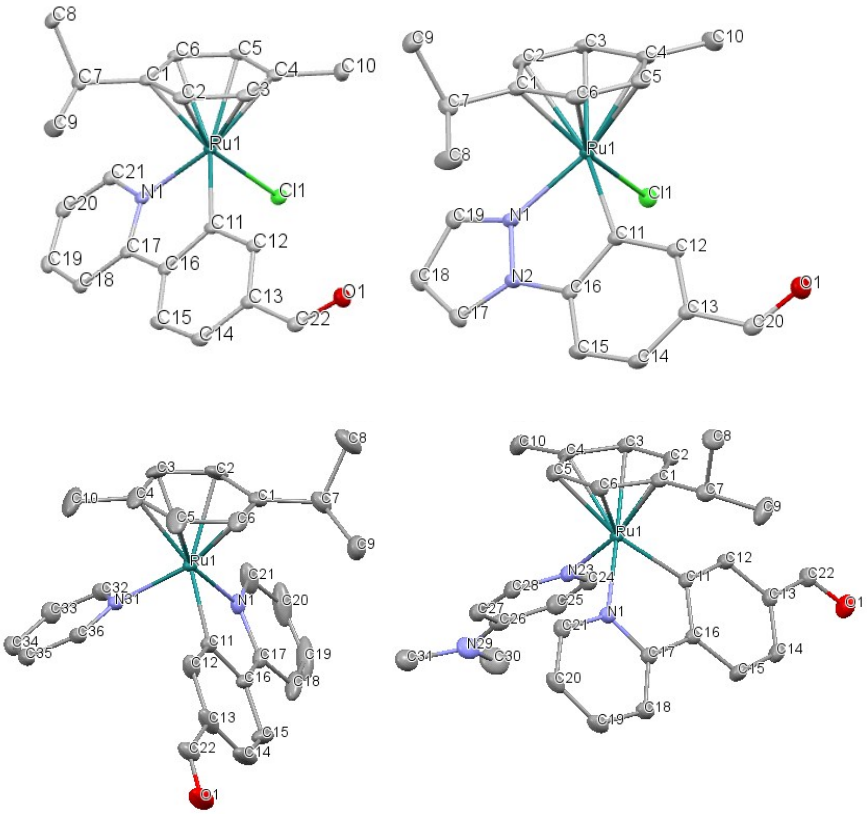

Figure S47. ORTEP diagrams of complexes **1a** and **1b** (upper row) and **2a** and **3a** (botton row) showing thermal ellipsoids at the 50% probability level.

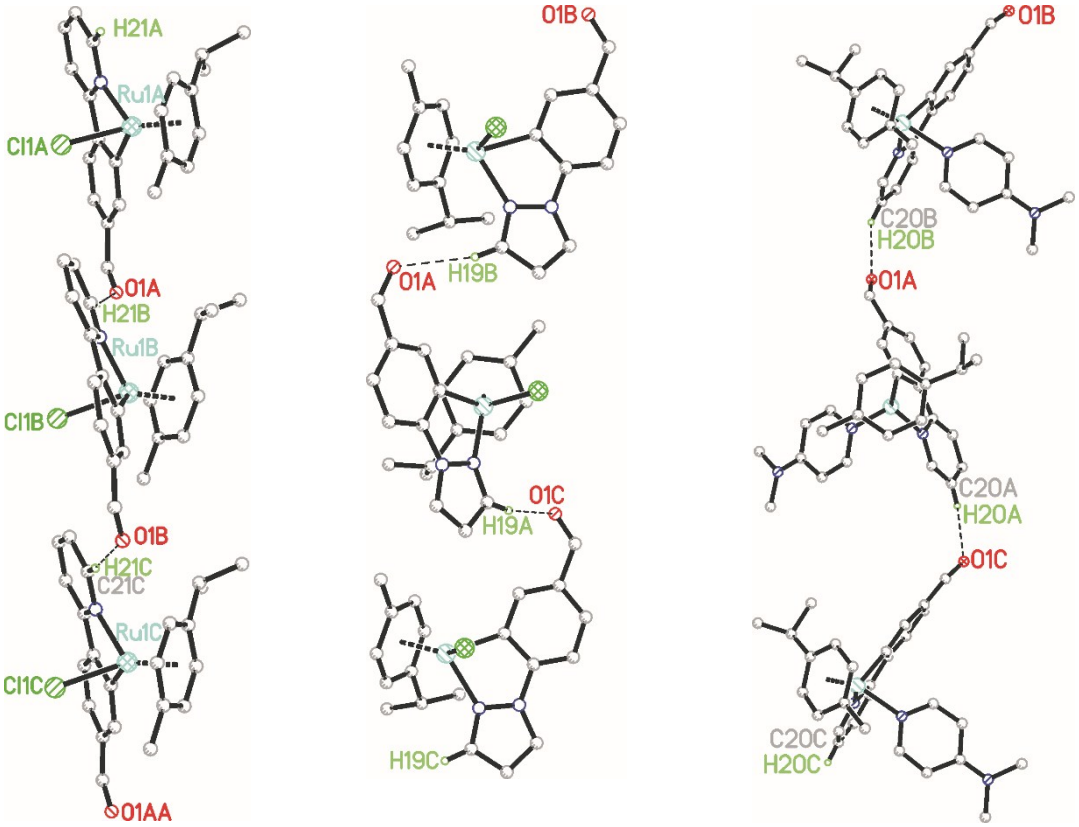

Figure S48. Schematic showing hydrogen bonding in complexes **1a** (left), **1b** (center), and **3a** (right).

Table S3. Hydrogen bonds for **1a** [Å and °]

D-H...A	d(D-H)	d(H...A)	d(D...A)	<(DHA)
C(21)-H(21)...O(1)#1	0.95	2.43	3.3547(17)	164.7

Symmetry transformations used to generate equivalent atoms:
#1 x+1/2,-y+1/2,z+1/2

Table S4. Hydrogen bonds for **1b** [Å and °]

D-H...A	d(D-H)	d(H...A)	d(D...A)	<(DHA)
C(17)-H(17)...Cl(1)#1	0.95	2.70	3.6273(15)	166.2
C(18)-H(8)...Cl(1)#2	0.95	2.80	3.7149(15)	162.0
C(19)-H(19)...O(1)#2	0.95	2.56	3.4821(18)	163.6

Symmetry transformations used to generate equivalent atoms:
#1 -x+3/2,y+1/2,-z+1/2 #2 x+1/2,-y+1/2,z+1/2

Table S5. Hydrogen bonds for **2a** [Å and °]

D-H...A	d(D-H)	d(H...A)	d(D...A)	<(DHA)
C(21)-H(21)...O(2B)#1	0.95	2.17	2.994(4)	145.1
C(32)-H(32)...O(2)#1	0.95	2.38	3.244(4)	151.0
C(32)-H(32)...O(2B)#1	0.95	2.33	3.243(4)	162.2
C(35)-H(35)...O(2)#2	0.95	2.55	3.387(4)	147.3
C(36)-H(36)...O(4)#2	0.95	2.32	3.149(4)	146.1
C(36)-H(36)...O(4B)#2	0.95	2.47	3.196(4)	133.3

Symmetry transformations used to generate equivalent atoms:
#1 -x+1/2,y-1/2,-z+1/2 #2 -x+1,-y+1,-z+1

Table S6. Hydrogen bonds for **3a** [Å and °]

D-H...A	d(D-H)	d(H...A)	d(D...A)	<(DHA)
C(20)-H(20)...O(1)#1	0.95	2.46	3.303(2)	148.2

Symmetry transformations used to generate equivalent atoms:
#1 x+1/2,-y+3/2,z-1/2

Reaction with human serum albumin (HSA)

Procedures fluorescence Quenching Studies. The stock solutions of proteins (6.5×10^{-6} mol L^{-1}) were prepared by dissolving the solid HSA in 50 mM Tris-HCl, 100 mM NaCl buffer of pH 7.4 and stored at 0–4 °C in the dark for about a week. The concentrations of HSA were determined from optical density measurements, using the values of molar absorptivity of ε_{278} = 36 000 M^{-1} cm^{-1}.[3]

Quantitative analyses of the interaction between complexes **1a,b** – **3a,b** and HSA were performed by fluorimetric titration. A 3.0 mL portion of aqueous solution of protein (5×10^{-6} mol L^{-1}) was titrated by successive additions of complex solution (to give a final concentration of 32.5 $\times 10^{-6}$ mol L^{-1}). Titrations were done manually by using a micropipette. For every addition, the mixture solution was shaken and allowed to stand for 5 min and then the fluorescence intensities were measured with an excitation wavelength of 295 nm and emission wavelengths in the interval 300−550 nm. The width of the excitation and emission slit was set to 5 nm. In the meantime, the synchronous fluorescence intensity of the mixture solution was measured at $\Delta\lambda$ = 15 nm and $\Delta\lambda$ = 60 nm, respectively.

The fluorescence quenching constant (K_{SV}) values were calculated from Stern-Volmer equation using an F^0/F *versus [M]* plot (Table S7, Figure S49) [4,5,6]

Table S7. Parameters obtained from HSA interactions with the prepared complexes

Complex	K_{SV} (M^{-1})	K_q (M^{-1} s^{-1})	K_B (M^{-1})	*n*
1a	4.9 x 10^4	x 10^{12}	2.0 x 10^4	0.92
1b	5.1 x 10^4	x 10^{12}	4.0 x 10^4	0.99
2a	5.9 x 10^4	x 10^{12}	2.2 x 10^4	0.91
2b	6.4 x 10^4	x 10^{12}	2.5 x 10^4	0.91
3a*	1.5 x 10^5	x 10^{12}	4.7 x 10^4	0.92
3b	1.2 x 10^5	x 10^{12}	4.4 x 10^4	0.91

* K_{SV} value was calculated from F0/(F0-F) versus 1/[**3a**]

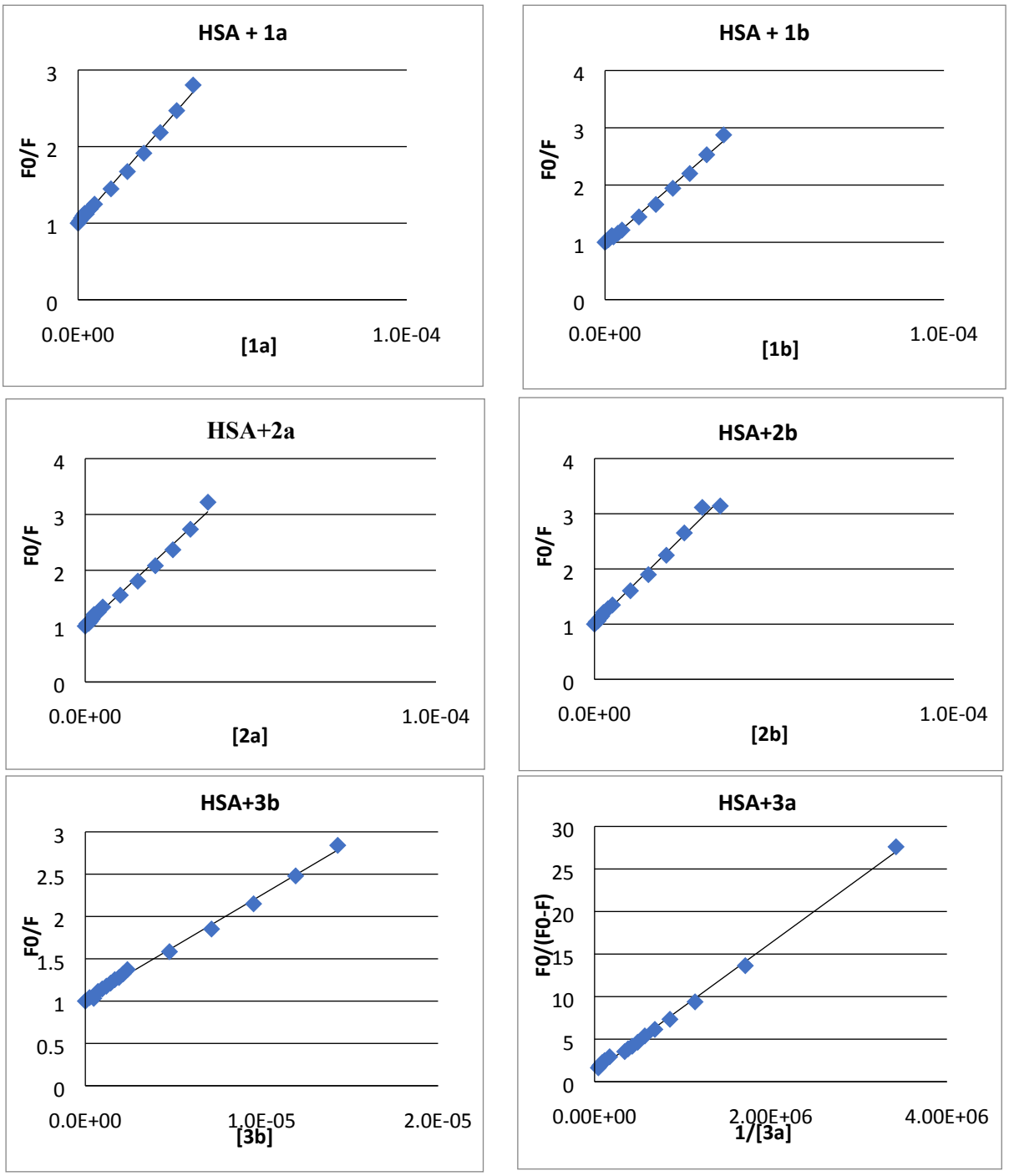

Figure S49. Stern-Volmer plots of protein fluorescence quenching.

The mechanism of quenching can be determined from changes in the electronic absorption spectrum of HSA in the presence of different amounts of the complexes. In **Figure S50** the spectrum of the HSA and its spectra in the presence of different amounts of the complexes **1a,b-3a,b** are shown. The intensity of the absorption decreases drastically in the presence of the complexes and the maximum underwent red shift, all this suggested a static mechanism of quenching.

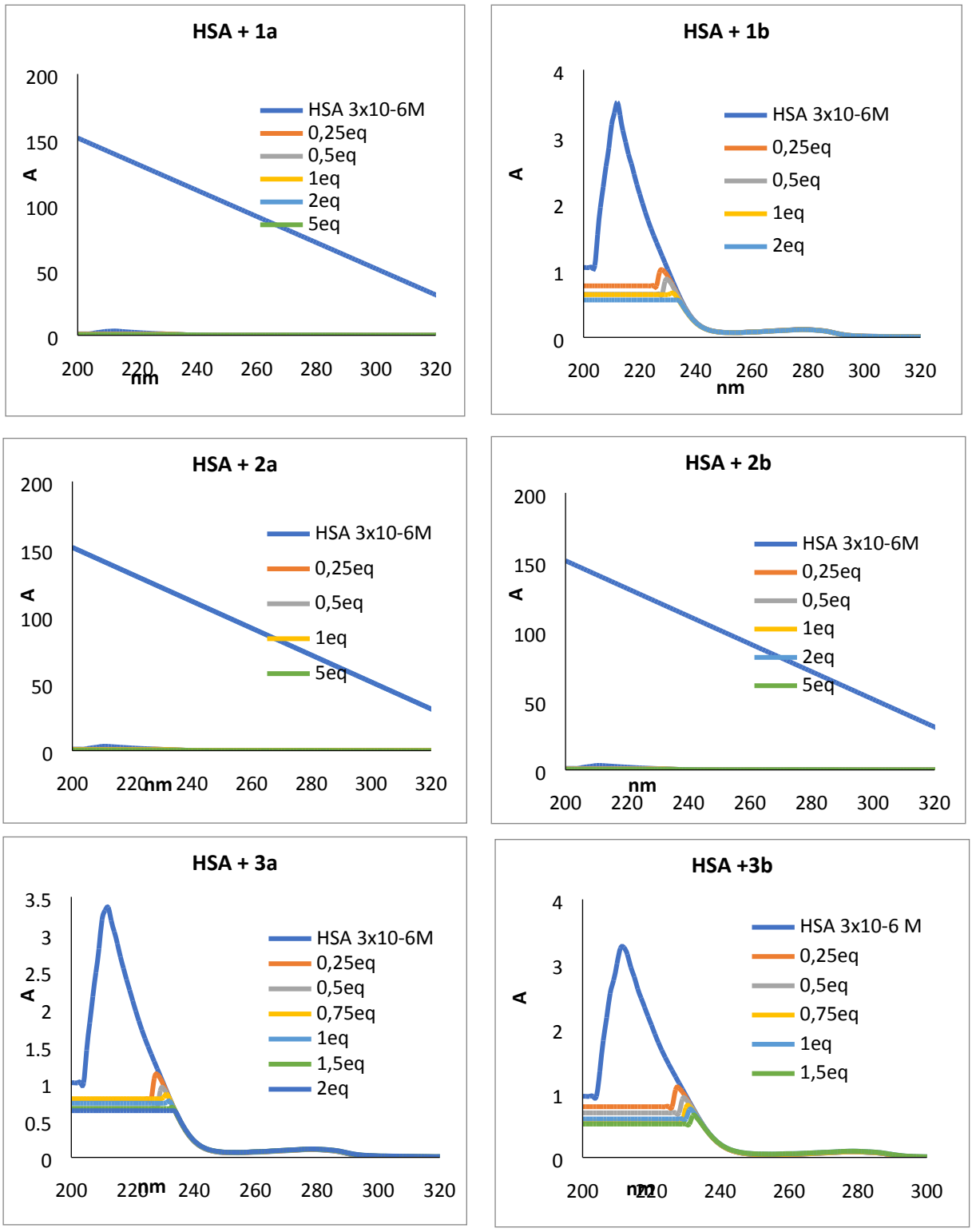

Figure S50. UV-VIS Absorption spectra of HSA = ($3x10^{-6}$ M) (blue), and of HSA with different concentration of complexes.

When small molecules bind independently to a set of equivalent sites on a macromolecule, the equilibrium between free and bound molecules is given by Scatchard equation (**Eq. 1**):

$$\log(F_0 - F)/F = \log K + n \log[Q] \qquad \textbf{(Eq. 1)}$$

where K is the observed binding constant to a site, n is the number of binding sites per HSA and [Q] the concentration of complex. The data at 298 K were handled in this way and the linear plot of log (F_0- F)/F as a function of log [Q] is shown in Figure S51.

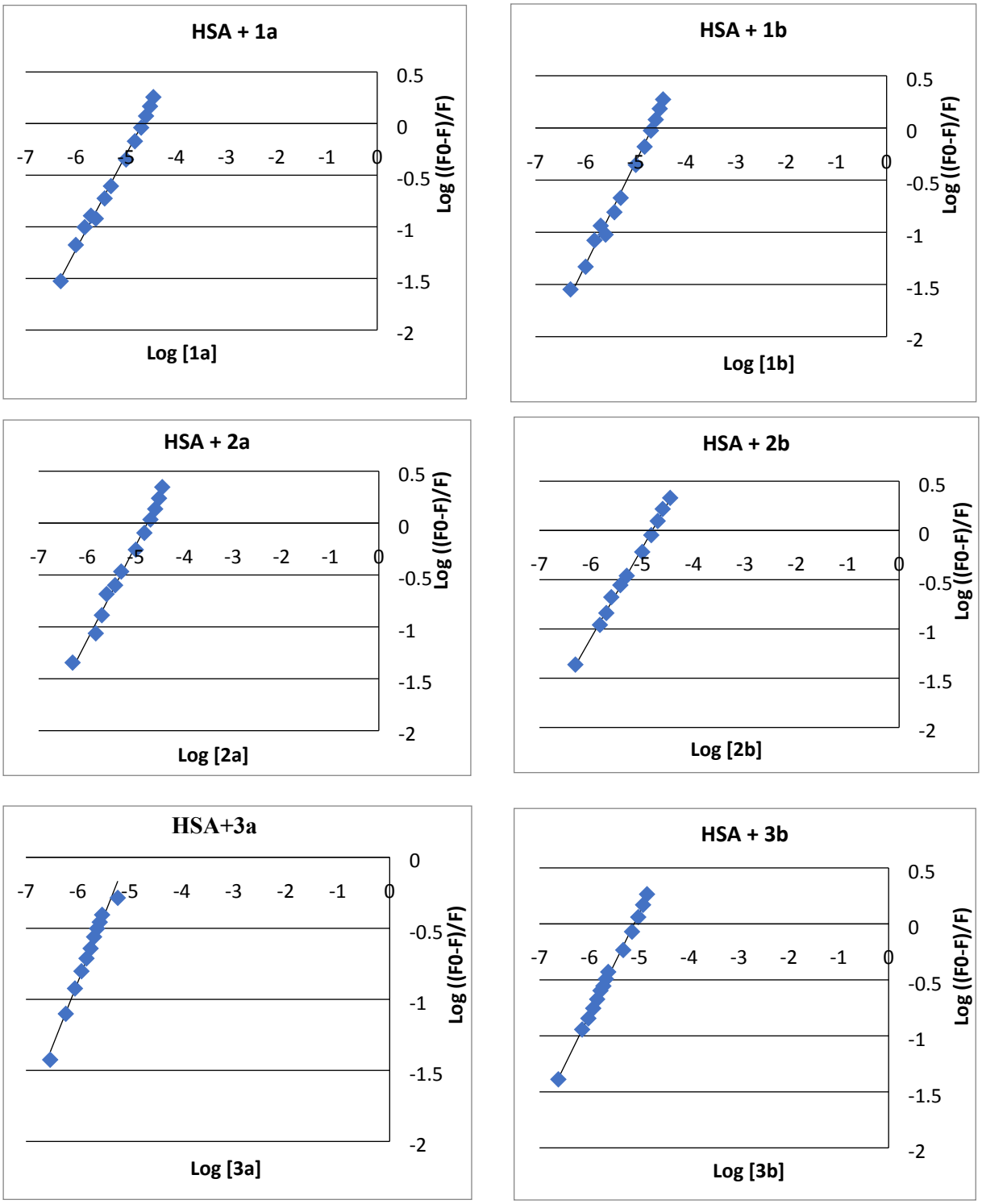

Figure S51. Stern-Volmer plots of protein fluorescence quenching.

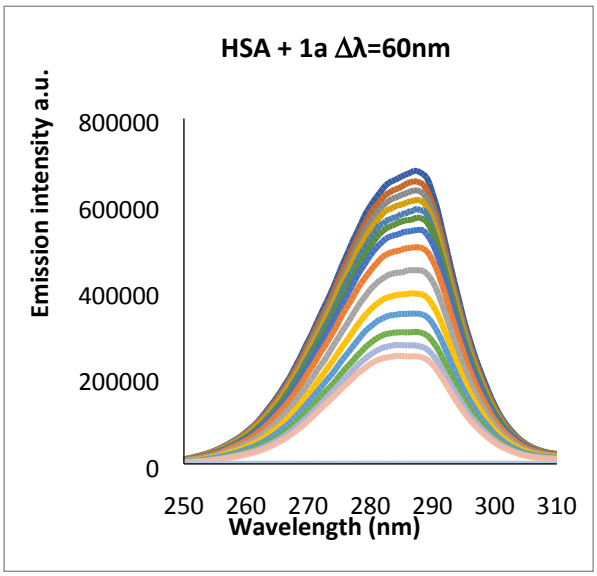
HSA + 1a Δλ=60nm
Emission intensity a.u.
800000
600000
400000
200000
0
250 260 270 280 290 300 310
Wavelength (nm)

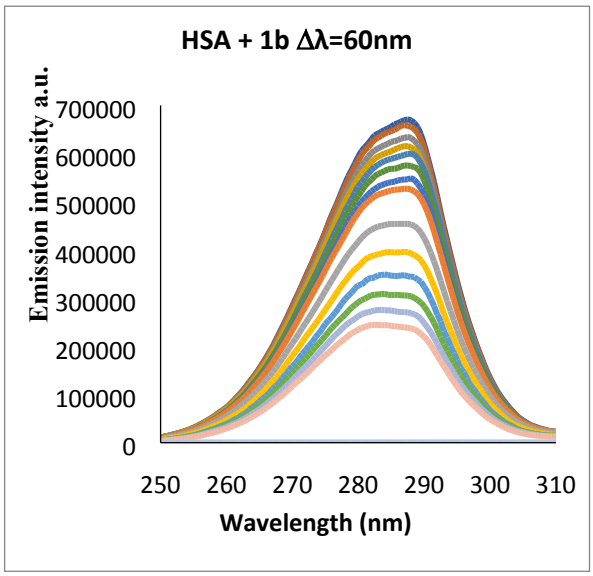
HSA + 1b Δλ=60nm
Emission intensity a.u.
700000
600000
500000
400000
300000
200000
100000
0
250 260 270 280 290 300 310
Wavelength (nm)

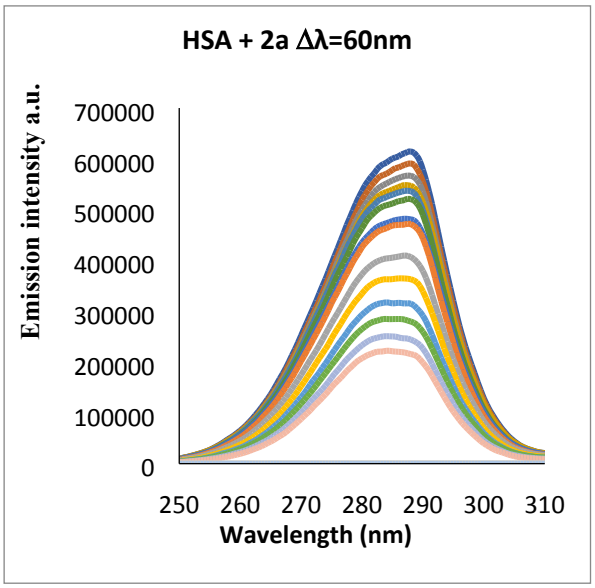
HSA + 2a Δλ=60nm
Emission intensity a.u.
700000
600000
500000
400000
300000
200000
100000
0
250 260 270 280 290 300 310
Wavelength (nm)

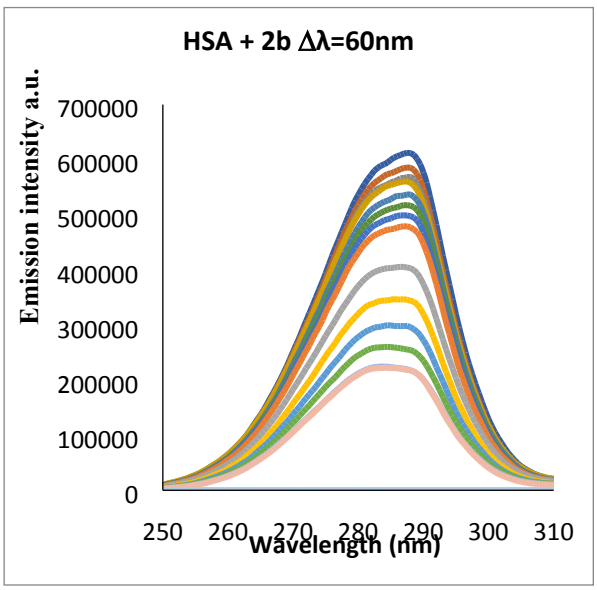
HSA + 2b Δλ=60nm
Emission intensity a.u.
700000
600000
500000
400000
300000
200000
100000
0
250 260 270 280 290 300 310
Wavelength (nm)

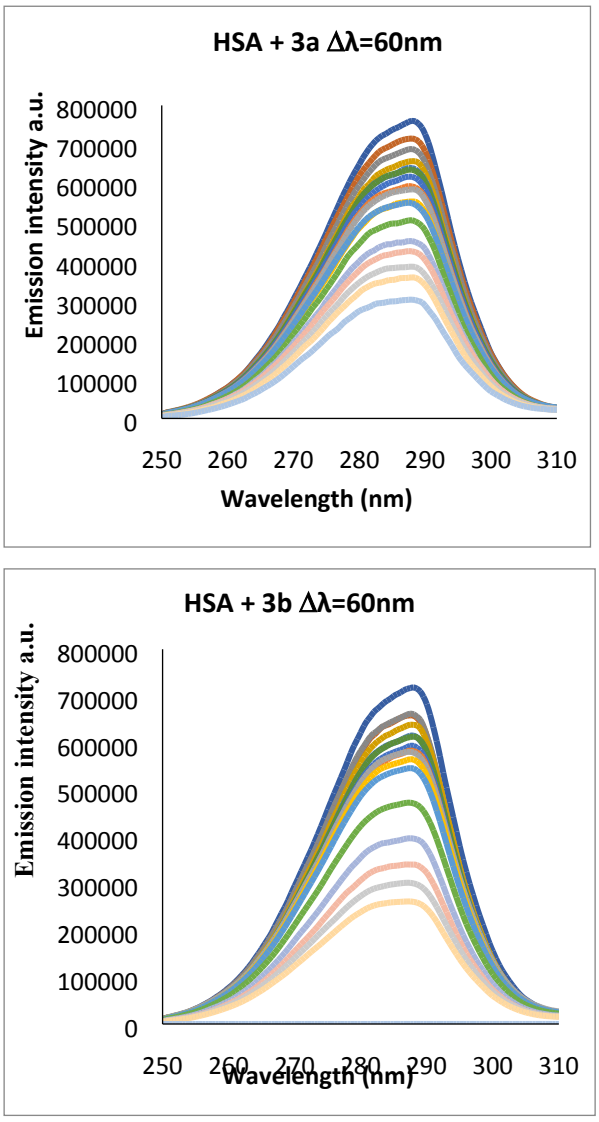

Figure S52. Synchronous spectra of HSA as a function of concentration of complexes when Δλ = 60 nm.

Cell lines and culture

Human ovarian carcinoma A2780 and A2780cisR cell lines were grown in RPMI-1640 supplemented with 10% fetal bovine serum (FBS) and 2 mM L-glutamine. Breast cancer cells, MCF-7, and the non-tumorigenic kidney cells, BGM, were grown in DMEM containing 1 g/L glucose supplemented with 10% final concentration of FBS, 2 mM L-glutamine and 0.1 mM non-essential amino acids. Non-tumorigenic chinese hamster ovary cells, CHO, were grown in FK-12 medium supplemented with 10 % FBS and 2mM L-glutamine. The acquired resistance of A2780cisR cells was maintained by supplementing the medium with 1 μM cisplatin every second passage to cell culture flasks. All cell lines were cultured in a humidified incubator at 310 K in a 5% CO_2 atmosphere and subcultured 2–3 times a week with an appropriate density for each cell line. The cells lines were confirmed to be mycoplasma-free using Hoechst DNA staining method [7]. The maximum % of DMSO used in cell experiments was 0.4 (except for cisplatin, water diluted).

Cytotoxicity assays

Cell viability was determined using a 3-(4,5-dimethylthiazo-2-yl)-2,5-diphenyl-tetrazolium bromide (MTT)-based vitality assay upon exposure of the compounds. Cells were cultured in 96-well plates at a density of 5000 cells/well in complete medium and incubated for 24 h. Ruthenium complexes were added at the final concentration range of 0 to 80 μM in a volume of 100 μL per well and incubated for 48 h. Drug-containing medium was removed and 50 μL MTT (1 mg/mL) was added. After incubation of the cells for 4 h at 310 K, the MTT solution was removed and 100 μL DMSO was added to solubilize the formazan crystals formed in active cells. The absorbance was measured at 570 nm using a microplate reader (FLUOstar Omega) and the IC_{50} values were calculated based on the inhibitory rate curves using the next the equation (**Eq. 2**):

$$I = \frac{I_{max}}{1 + \left(\frac{IC_{50}}{C}\right)^n} \quad \textbf{(Eq. 2)}$$

Where I represent the percentage inhibition of viability observed, $Imax$ is the maximal inhibitory effect, IC_{50} is the concentration that inhibits 50% of maximal growth, C is the concentration of the compound and n is the slope of the semi-logarithmic dose-response sigmoidal curves. The non-linear fitting was performed using SigmaPlot 14.0 software. All compounds were tested at least in two independent studies with quadruplicate points.

Metal accumulation

The A2780 cells were seeded at $1 \cdot 10^6$ cells/well in 6-well plates in 1.8 mL of complete growth medium. After 24 h or incubation, the cells were treated with 2 μM of the tested compounds for additional 24 h. Cells were then trypsinized, counted and the pellets digested using Suprapur® nitric acid 30 % for 4 h. The amount of metal elements ruthenium and platinum was determined using Inductively Coupled Plasma Mass Spectrometry (ICP-MS).

Compound	**ng/10^6 cells**
1a	0.48 ± 0.14
1b	1.24 ± 0.17
2a	3.59 ± 0.89
2b	2.23 ± 0.75
3a	12.34 ± 1.29
3b	10.66 ± 1.56
CDDP	6.81 ± 0.83

Table S8. Cellular ruthenium and platinum accumulation in A2780 cancer cells after 24 h treatment with either 2 μM of **1a-3b** or cisplatin. Measurements indicate total cellular uptake of ^{101}Ru for tested compounds and ^{195}Pt for cisplatin.

Mitochondrial polarization assay

Mitochondrial membrane potential was evaluated with the fluorescent probe Rhodamine-123 (Sigma-Aldrich). A2780 cells in the density of $2 \cdot 10^4$ were seeded for 24 h in complete medium on 96-well plates, and then treated with various concentrations (0-20 μM) of **3a, 3b** or cisplatin for 24 h. Untreated cells contained maximal concentration of DMSO used in the treatment (0.4%). After the treatment, the cells were incubated with Rhodamine-123 dye (1 μM) for 15 min at room temperature and scanned using a FLUOstar Omega spectrofluorometer with excitation and emission wavelengths 488 nm and 530 nm, respectively. Alternatively, cells were treated as indicated and subsequently imaged using Leica SP2 fluorescence microscopy. Experiments were repeated at least in duplicate using triplicate points per concentration level.

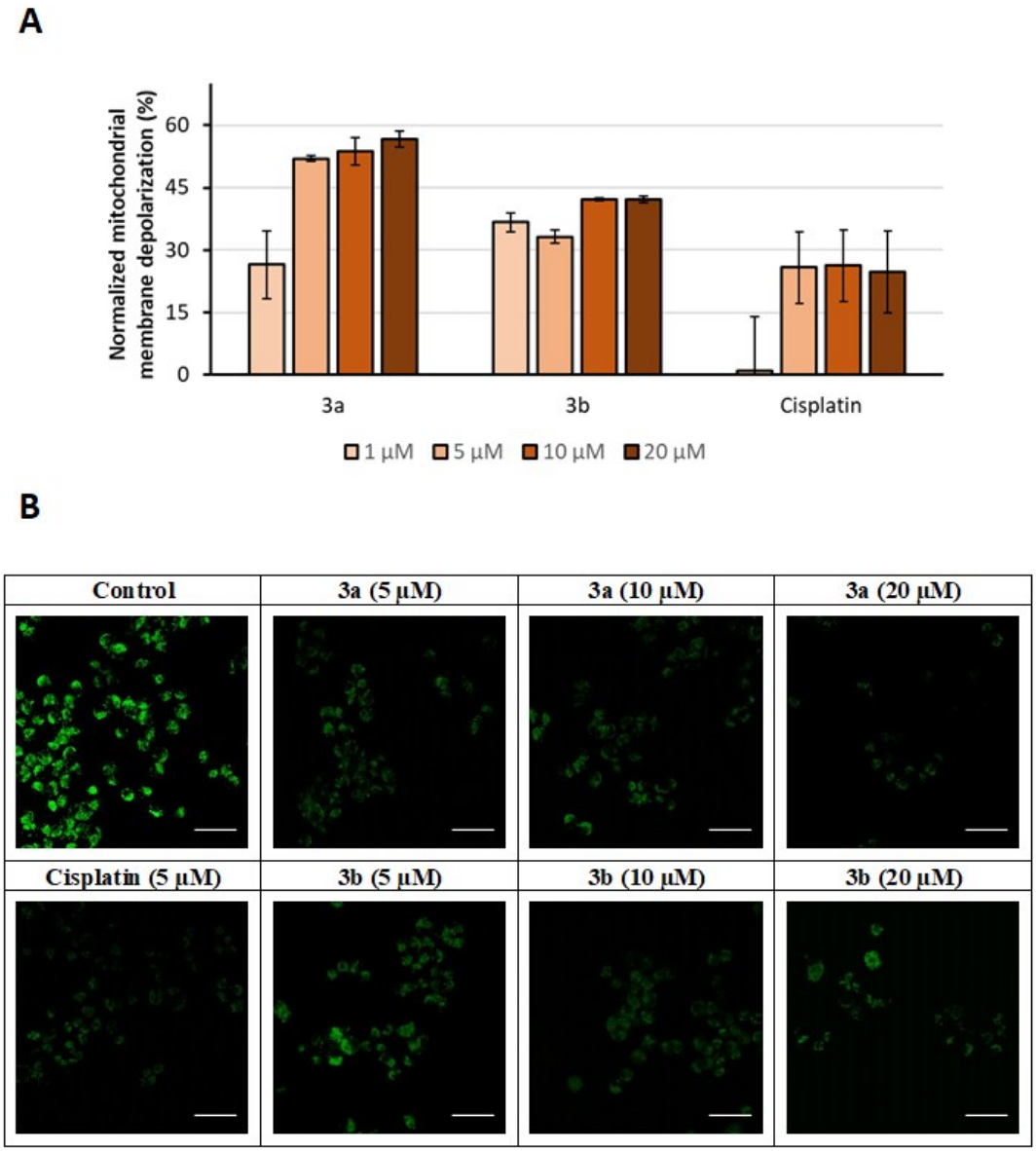

Figure S53. Effect of ruthenium complexes **3a** and **3b** on mitochondrial membrane potential using Rhodamine-123 staining. Cisplatin was used for comparative purposes. (A) Normalized mitochondrial depolarization of A2780 cells treated for 24 h at the indicated concentrations where untreated control cells were taken as 0% depolarization. Data are presented as mean ± SD. (B) Fluorescence microscopy images of A2780 cells Rhodamine-123 stained cells upon treatment with ruthenium complexes.

Apoptotic induction assay

The impact on apoptosis or necrosis of the ruthenium complexes on A2780 cells was evaluated using the FITC-Annexin V/Propidium Iodide (PI) dual staining method. Briefly, A2780 cells were seeded in 12-well plates at a density of $2 \cdot 10^5$ cells/well and incubated overnight. Ruthenium complexes or cisplatin were added at indicated concentrations for 24 h. The cells were then harvested, washed with PBS, centrifuged and the pellets were resuspended in 185 µL binding buffer. Then, 15 µL of FITC-Annexin-V/PI solution 1:2 were added and the resuspended cell solution was left at room temperature in the dark for 15 min. Cells were analyzed by flow cytometry (Beckman CoulterEpics XL) and a total of 10000 events were acquired in each sample, registering at 620 and 525 nm for PI and Annexin V, respectively, λ_{exc} = 488 nm. Data were analyzed using FlowingSoftware version 2.5.1.

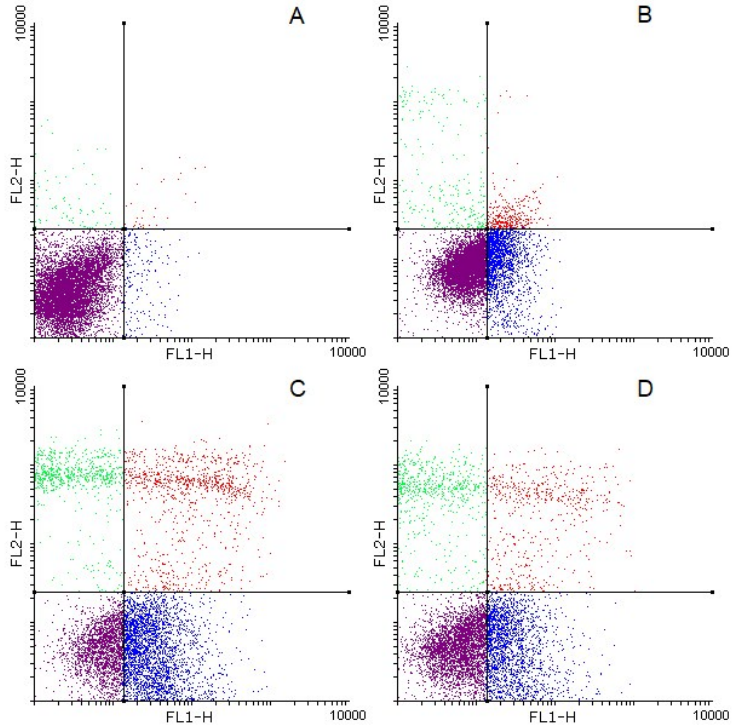

Figure S54. Density plots of A2780 cells after 24 h treatment with **3a** (C) **3b** (D) or cisplatin (B) at 10 µM determined using Annexin V/PI by flow cytometry. Control cells (A) contained maximal DMSO concentration used in treatments (0.4%). FL1-H channel indicates Annexin V stained cells whereas FL2-H channel measures PI-positive cells.

Fluorescence detection of Caspase 3/7 activation

The A2780 cells were seeded at $1.2 \cdot 10^5$ cell/well in 24-well plates. The following day, the ruthenium compounds (10 µM) or cycloheximide (500 µM) were added alongside with 8 µM of CellEvent™ Caspase-3/7 Green Detection Reagent. Cells were imaged by fluorescence microscopy at 12, 24 and 48 h after treatment using λ_{exc} = 500 nm.

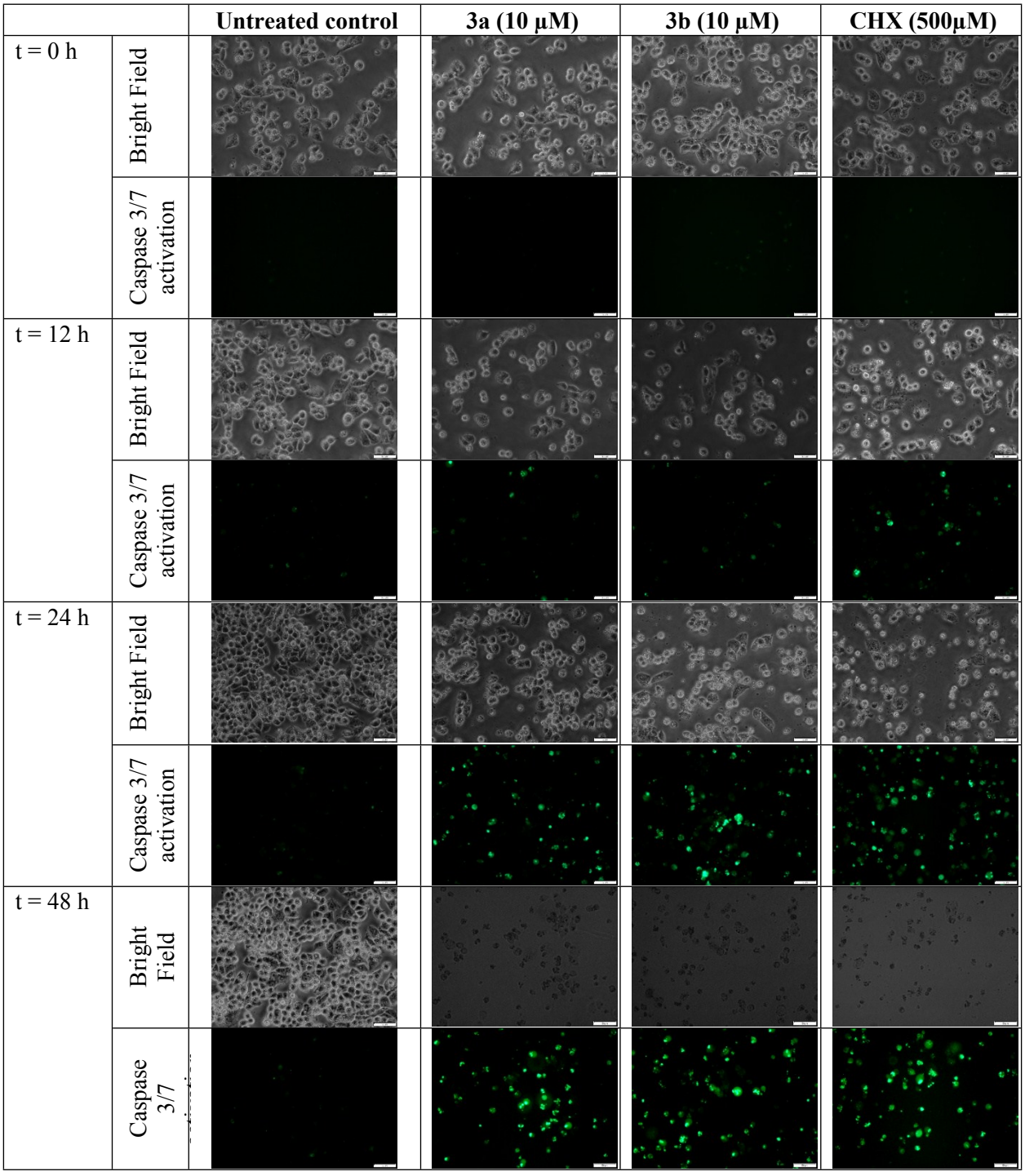

Figure S55. Caspase 3/7 activation upon treatment with ruthenium complexes **3a** and **3b** or cycloheximide over a span of 48 hours. Scale bar = 50 µM

ROS induction assay

A2780 cells in the density of 2 x 10^4 cells/well were seeded for 24 h in 200 μL per well RPMI medium without Phenol Red on 96-well black plates. Cells were then washed with PBS and incubated with 10 μM 2′,7′-dichlorodihydrofluorescein diacetate (DCFH-DA) for 30 min at 310 K. After incubation, DCFH-DA solution was removed, and ruthenium compounds diluted in RPMI without phenol red were added to the cells at appropriate concentrations for 2 hours. Fluorescence of DCF product was measured using FLUOstar Omega spectrofluorometer. Experiments were repeated in triplicate with quadruplicate points. Alternatively, 2 x 10^5 A2780 cells were seeded on 100 nm petri dishes, treated as described above and imaged using Lecia SP2 fluorescence microscopy.

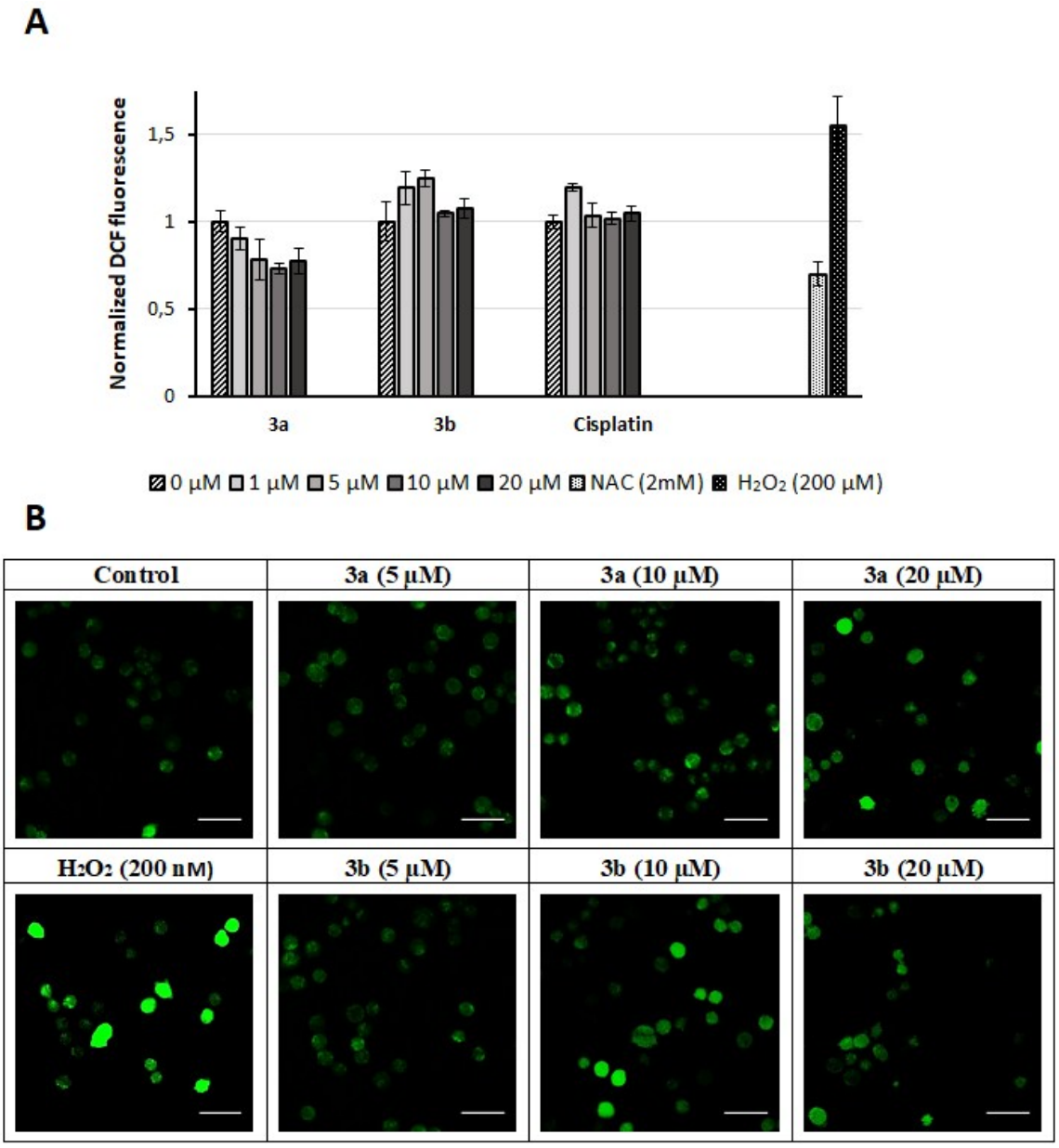

Figure S56. ROS formation analysis of A2780 cells upon 2 h exposure of **3a, 3b** or cisplatin. Cells were then stained with 10 µM DCFH-DA during 45 min. (A) Normalized DCF fluorescence intensity measurements after treatment. Statistical data are shown as mean ± SD (n = 3). Untreated cells (0 µM) were used as negative control, N-acetyl-cysteine (NAC) was used as a positive control for ROS scavenging whereas hydrogen peroxide (H_2O_2) was used as a positive control for ROS induction. (B) Fluorescence microscopy images of ROS formation after treatment. Scale bar = 40 µm.

Real-time cell electronic sensing

The real-time cell analyzer (RTCA) equipment (xCELLigence RTCA SP instrument, Roche) was calibrated for the background impedance with fresh RPMI 1640 medium (100 µL). A2780 cells were added at a density of 8000 and 4000 cells per well, respectively, and were incubated for 24 h at 37 °C under a humidified 5 % CO2 atmosphere. Subsequently, the cells were treated with tested compounds. Cell-sensor impedance called the cell index is defined as (Eq. 3):

$$\text{Cell index} = \frac{(R_t - R_b)}{15} \quad \text{(Eq. 3)}$$

in which Rt is the impedance of the cells at defined time points, and Rb is the background impedance of the culture medium. Impedance was monitored for 5 min sweeps for the duration of the experiment. Cell index was normalized at the time of treatment (24 h). Each sample was plated on the E-plate as quadruplicate. The concentrations of treated compounds in the media used for treatment were verified by flameless atomic absorption spectroscopy (FAAS).

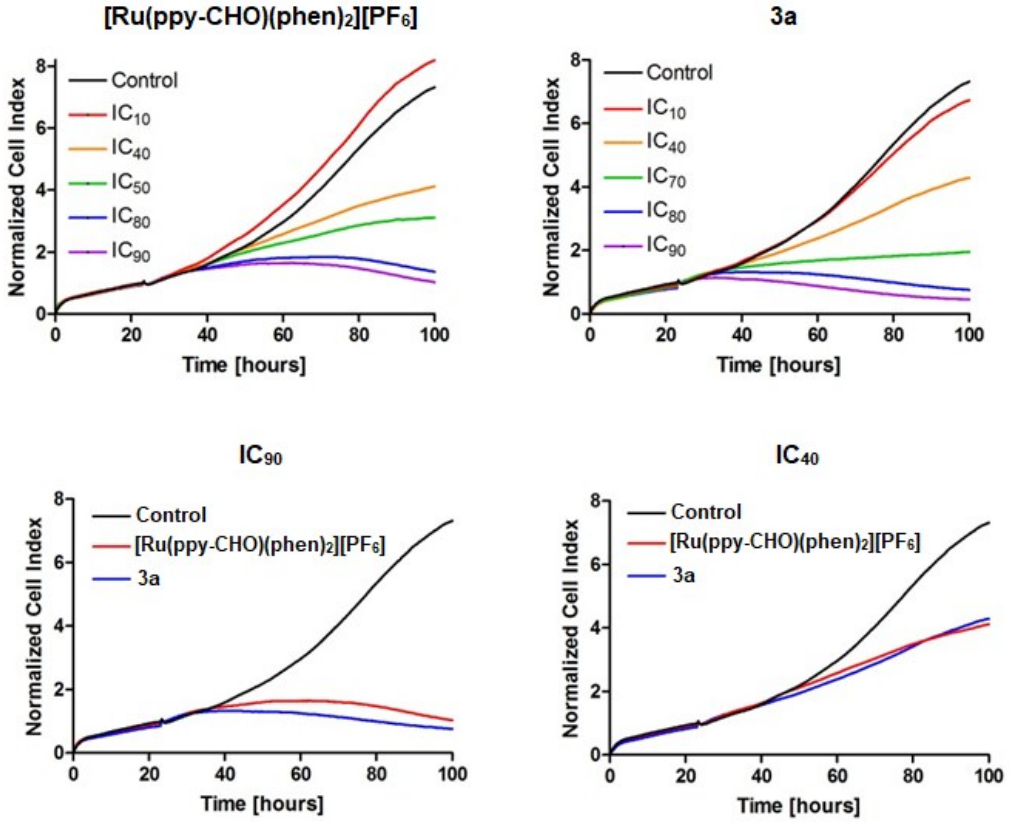

Figure S57. Interaction of RuL1 (top right panel) and **3a** (top left panel) with A2780 cells monitored by a real-time cell analyzer (RTCA). Bottom panels: A comparison of RTCA profiles found for **[Ru(ppy-CHO)(phen)$_2$][PF$_6$]** and **3a** in their equitoxic concentrations corresponding to IC_{90} (left) and IC_{40} (right). Before the treatment, the cells were allowed to grow and adhere to microelectrodes for 24 h. Incubations were performed in quadruplicate with 10 000 cells per well using inhibitory drug concentrations determined for 72 h of incubation in colorimetric cell viability assay.

Protein synthesis inhibition assay

Nascent protein synthesis was assayed using the Click-iT Plus O-propargyl-puromycin (OPP) Protein Synthesis Assay Kit (Invitrogen™) according to manufacture instructions. Briefly, A2780 cells were incubated at $1 \cdot 10^4$ cells/well in 96-well black plates for 24 h and treated with the ruthenium complexes or cycloheximide for 6 hours. Then 20 µM Click-iT OPP reagent for 30 min, fixed with 3.7% formaldehyde in PBS, permeabilized with 0.5% Triton X-100 and then stained with the Click-iT Plus OPP reaction cocktail containing Alexa Fluor 488 picolyl azide as instructed. Cells were then washed, counterstained with NuclearMask blue stain and imaged by confocal fluorescence microscopy. Alternatively, quantification of OPP labeling was measured using ClarioStar™ microplate reader.

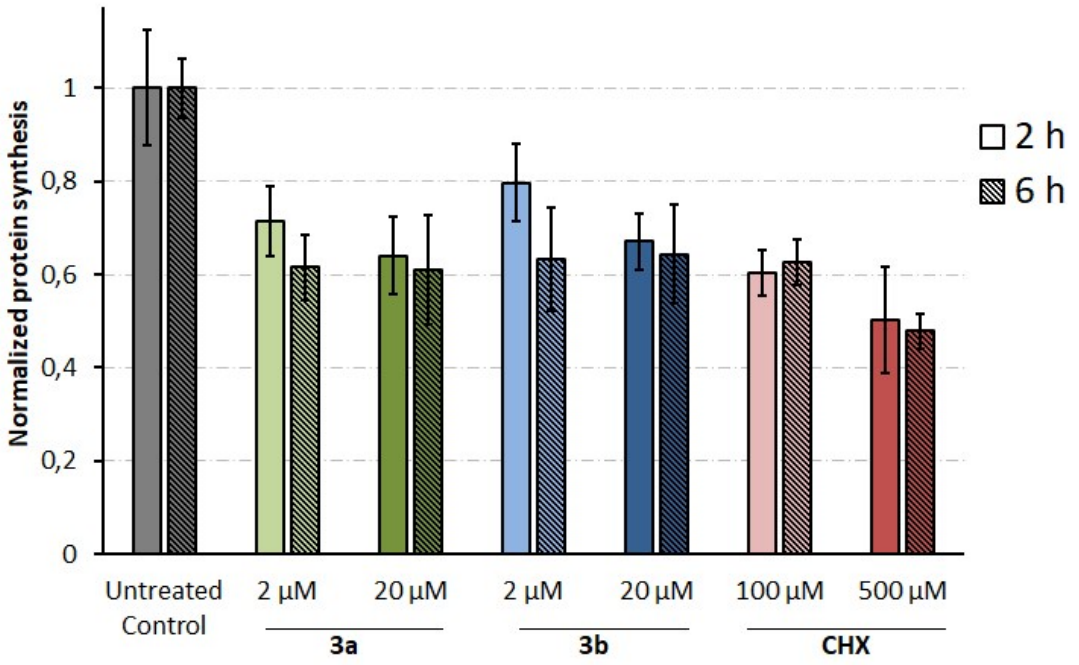

Figure S58. Effect of Ru complexes **3a** and **3b** on nascent protein synthesis at different concentrations after 2 or 6 hours of drug-exposure measured with OPP Click-It Alexa Fluor technology (Invitrogen™). Cycloheximide (CHX) was used as a positive control for protein synthesis inhibition

Flow cytometric cell cycle analysis

A2780 cells were seeded into 6-well plates at a density of $3 \cdot 10^5$ cells/well. Treatment with either DMSO alone or with 4 μM of **3a**, **3b** or cisplatin was added for 24 h. Then cells were trypsinized, fixed in ice-cold 75% ethanol for 1 h, treated with RNase 1 μg/mL, stained with 40 μg/mL PI for 30 min and analyzed using Beckman CoulterEpics cytometer (λ_{exc} = 488 nm and λ_{em} = 630).

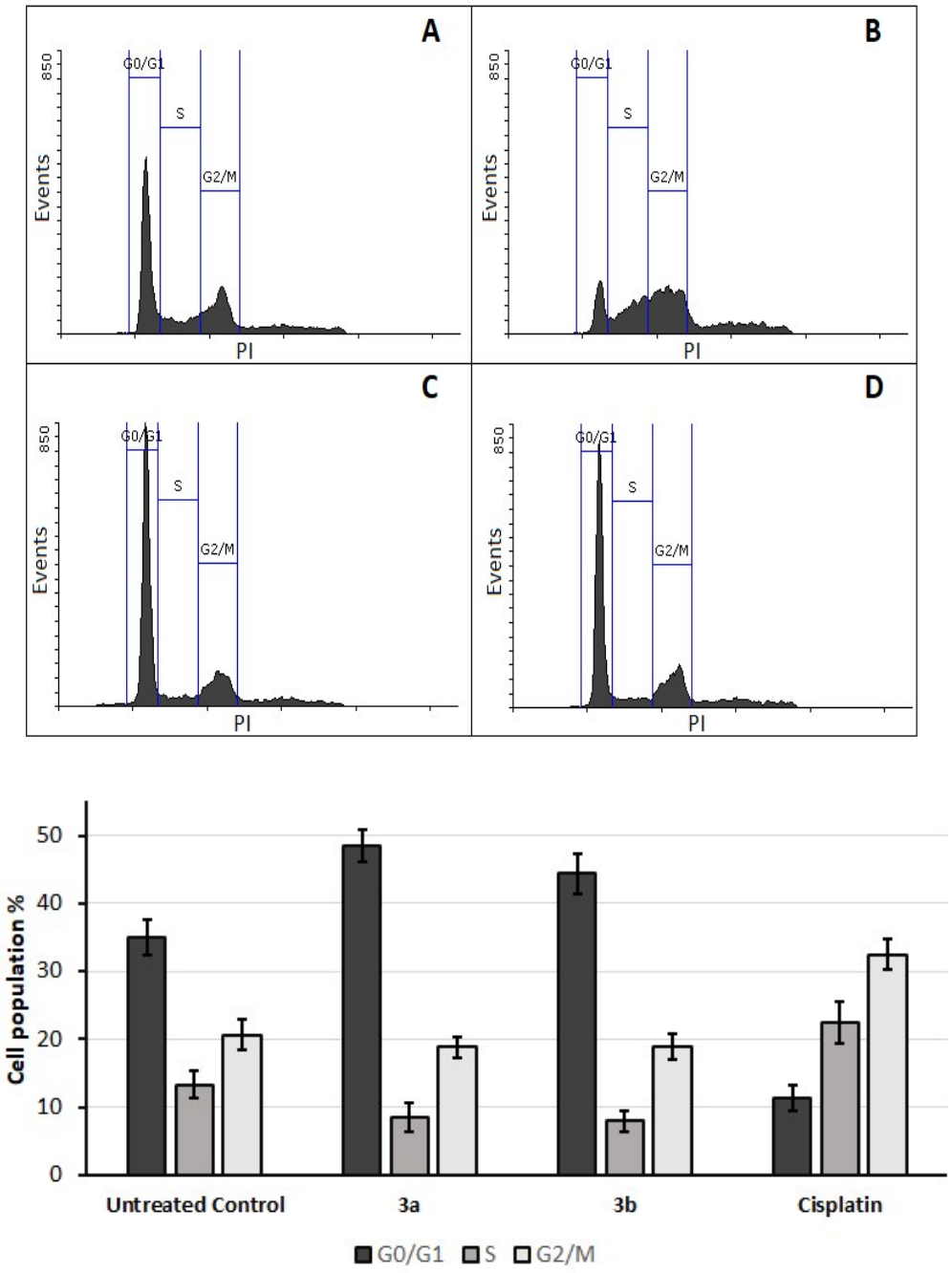

Figure S59. Flow cytometry analysis of cell cycle distribution of A2780 cancer cells performed by propidium iodide staining upon 4 μM exposure of **3a** (C), **3b** (D) or cisplatin (B) for 24 h. Control cells (A) were treated with the vehicle (DMSO 0.4%).

Quantitative-PCR (qPCR)

A2780 cells ($1.5x10^6$) were seeded in 60 mm culture dishes and treated with **3a** (20μM), **3b** (20μM) and CHX (500μM) for 6 h in complete medium. After that, cells were collected and ther RNA isolated using the NucleoSpin ARN kit (Macherey-Nagel, Düren,Germany), following the manufacturer instructions. RNA concentration was quantified using a spectrophotometer (Nanodrop 2000) and the samples stored at -80°C until use.

Reverse transcription (RT) reactions were conducted in three steps: 1) 0.5μg of RNA were diluted in 12.5 μl of RNase-free H2O and transferred into a PCR tube. Then, MIX 1 [1.5 μl of dNTPs (50nM, Invitrogen) and 5 μl of Random primers (50nM, ThermoFisher)] was added to the tube and samples were incubated for 5 min at 65°C in the thermal cycler and held at 4°C. 2) MIX 2 [6 μl of "first-strand" buffer 5X (Invitrogen), 3 μl of 0.1M DTT (Invitrogen) and 1 μl of RNaseOUT™ Recombinant (10777019, ThermoFisher) was added to the tube and incubated in the thermal cycler for 2 min at 37°C. 3) 1 μl M-MLV reverse transcriptase (28025013, ThermoFisher) was added to the tube and samples were incubated for 10 min at 25°C, 50 min at 37°C and 15 min at 70°C in the thermal cycler.

Real-time PCR was performed on a StepOnePlus™ Real-Time PCR System (ThermoFisher Scientific). The following TaqMan Gene Expression Assays (ThermoFisher) were used: CHAC1 (Hs00225520_m1), ATF3 (Hs00231069_m1) and CHOP (Hs00358796_g1). NOSIP (Hs00211028_m1) gene was included as endogenous control. The PCR reaction components were 2 μl of cDNA, 10 μl of TaqMan® Gene Expression Master Mix (4369016, ThermoFisher), 1μl of 20x TaqMan Gene Expression Assay and 7 μl RNAse-free water. The reaction was performed at 50°C for 2 min, at 95°C for 10 min and followed by 40 cycles of 95°C for 15 sec, 60°C for 15 s and 60°C for 1 min. Relative changes in gene expression were determined using the $2^{-\Delta\Delta cT}$ method [8] .

DNA damage assay: pH2AX detection

DNA damage in response to the complexes **3a** and **3b** was evaluated by flow cytometry as described previously [9]. 1.5 x 10^5 A2780 cells were seed in 12-well plate and treated with **3a** (20 μM), **3b** (20 μM), CHX (500 μM) and Etoposide (20 μM) as positive control, for 6 h. After that, cells were collected, washed twice with cold PBS and fixed in 50 μl 0.2% PFA for 5 min. Then, 150 μl of Block-9 buffer containing the anti-pH2AX (ser 139) FITC-conjugated antibody (16-202A, Millipore) at 0.6 μg/ml were added to the samples and incubated at 4°C for 3 h while protected from light. The stained cells were analyzed using the Guava EasyCyte flow cytometer and the InCyte Software(Millipore).

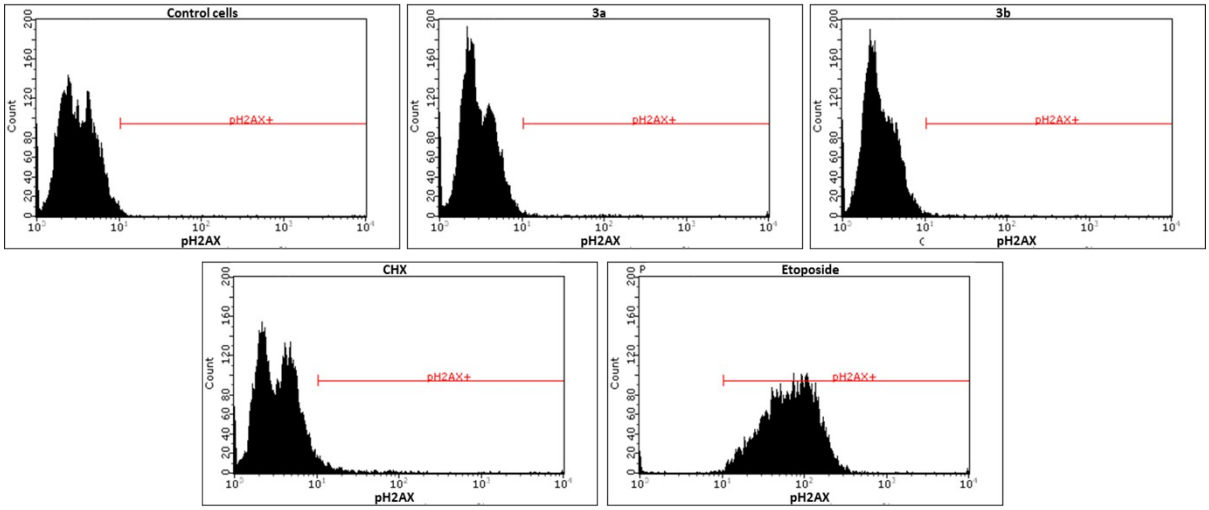

Figure S60: Effect of Ru complexes on DNA damage after 6 hours of treated measured by changes in gamma-H2AX phosphorylation. Cycloheximide (CHX) was used as a positive control for protein synthesis inhibition and Etoposide as positive control for DNA damage.

Superoxide levels

Flow cytometry measurement of ROS levels was performed using the specific superoxide indicator dihydroethdium (DHE) (Molecular Probes, D11347). 1.5x 10^5 A2780 cells were seeded in 12-well plate dishes and treated with **3a**, **3b** and CHX for 6 h. After that, cells were collected, washed twice with cold PBS and incubated with DHE (3.17 mM) for 20 minutes on ice. Stained cells were analyzed on the Guava EasyCyte flow cytometer (Millipore) with the InCyte software.

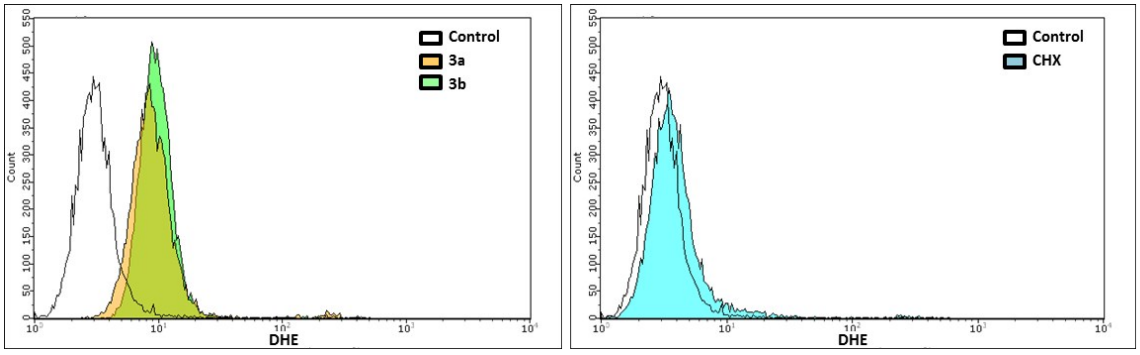

Figure S61: Measurements of superoxide in A2780 cells induced by 3a, 3b or CHX after 6 h of treatment. Cells were then stained with DHE during 20 min and analyzed by flow cytometry.

References

1. G.M. Sheldrick (2015) "Crystal structure refinement with SHELXL", *Acta Cryst.,* C71, 3-8 (Open Access)

2. G. M. Sheldrick, *Acta Crystallogr. Sect. A* 2018, **64**, 112.

3. J. R. Lakowicz, *Principles of Fluorescence Spectroscopy*, 3rd ed., Springer: New York, 2006.

4. N. Ibrahim, H. Ibrahim, S. Kim, J.-P. Nallet, F. Nepveu, *Biomacromolecules* **2010**, *11*, 3341−3351.

5. L. Shang, Y. Z. Wang, J. G. Jiang, S. J. Dong, *Langmuir* **2007**, *23*, 2714−2721.

6. F. Samari, B. Hemmateenejad, M. Shamsipur, M. Rashidi, H. Samouei, *Inorg. Chem*. **2012**, *51*, 3454−3464.

7. Chen, T. R. (1975) Microscopic demonstration of mycoplasma contamination in cell cultures and cell culture media. *TCA Manual 1*, 229–232

8. M. W. Pfaffl, G. W. Horgan and L. Dempfle*, Nucleic Acids Res*., **2002**, *30*, e36

9. A. Muslimovic, I. H. Ismail, Y. Gao and O. Hammarsten, *Nat. Protoc*., **2008**, *3*, 1187–1193